Journal of Computational Physics 259 (2014) 358–389

Contents lists available at ScienceDirect

Journal of Computational Physics

www.elsevier.com/locate/jcp

The generalized Riemann problems for compressible fluid flows: Towards high order ☆

Jianzhen Qian [a], Jiequan Li [b,*], Shuanghu Wang [a,c]

[a] Institute of Applied Physics and Computational Mathematics, Beijing 100088, PR China
[b] School of Mathematical Science, Beijing Normal University, Beijing 100875, PR China
[c] Key Laboratory of Computational Physics, Institute of Applied Physics and Computational Mathematics, Beijing 100088, PR China

ARTICLE INFO

Article history:
Received 30 January 2013
Received in revised form 21 November 2013
Accepted 2 December 2013
Available online 11 December 2013

Keywords:
Generalized Riemann problem
GRP solver
Generalized Riemann invariants

ABSTRACT

The generalized Riemann problems (GRP) for nonlinear hyperbolic systems of balance laws in one space dimension are now well-known and can be formulated as follows: Given initial data which are smooth on two sides of a discontinuity, determine the time evolution of the solution near the discontinuity. In particular, the GRP of $(k+1)$th order high-resolution is based on an analytical evaluation of time derivatives up to kth order, which turns out to be dependent only on the spatial derivatives up to kth order. While the classical Riemann problem serves as a primary "building block" in the construction of many numerical schemes (most notably the Godunov scheme), the analytic study of GRP will lead to an array of "GRP schemes", which extend the Godunov scheme. Currently there are extensive studies on the second-order GRP scheme, which proves to be robust and is capable of resolving complex multidimensional fluid dynamic problems (Ben-Artzi and Falcovitz, 2003 [4]). In this paper, we provide a new approach for solving the GRP for the compressible flow system towards high order accuracy. The derivation of second-order GRP solver is more concise compared to those in previous works and the third-order GRP (or quadratic GRP) is resolved for the first time. The latter is shown to be necessary through numerical experiments with strong discontinuities. Our method relies heavily on the new treatment of rarefaction waves. Indeed, as a main technical step, the "propagation of singularities" argument for the rarefaction fan, is simplified by deriving the linear ODE systems for the "evolution" of "characteristic derivatives", in the x–t coordinates, for generalized Riemann invariants. The case of sonic point is incorporated into a general treatment. The accuracy of the derived GRP solvers is justified and numerical examples are presented for the performance of the resulting schemes.

1. Introduction

This paper considers the *generalized Riemann problem* (GRP) for the system governing the quasi-1-D compressible flow in a duct of variable cross section

$$\frac{\partial}{\partial t}U + A(x)^{-1}\frac{\partial}{\partial x}\big[A(x)F(U)\big] + \frac{\partial}{\partial x}G(U) = 0,$$

☆ Jianzhen Qian is supported by the Postdoctoral Science Foundation of China (2012M510366); Jiequan Li is supported by NSFC (91130021, 11371063, 11031001), the Doctoral Program from Educational Ministry (20130003110004), the BNU Innovation Program (2012LZD08) and an open project from the Institute of Applied Physics and Computational Mathematics, Beijing; Shuanghu Wang is supported by NSFC (91130021).

* Corresponding author.
E-mail addresses: qianjzmath@gmail.com (J. Qian), jiequan@bnu.edu.cn (J. Li), wang_shuanghu@iapcm.ac.cn (S. Wang).

0021-9991/$ – see front matter
http://dx.doi.org/10.1016/j.jcp.2013.12.002

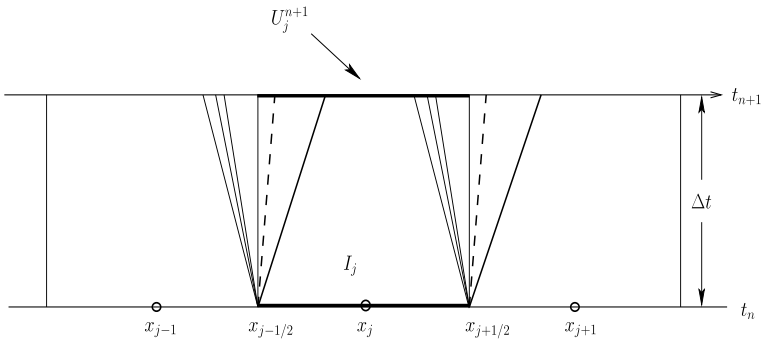

Fig. 1.1. Illustration for a control volume.

$$U=\begin{pmatrix}\rho\\ \rho u\\ E\end{pmatrix},\qquad F(U)=\begin{pmatrix}\rho\\ \rho u^2+p\\ (E+p)u\end{pmatrix},\qquad G(U)=\begin{pmatrix}0\\ p\\ 0\end{pmatrix}. \tag{1.1}$$

Here, the variables ρ, u, e are the density, velocity and internal energy, respectively, $p=p(\rho,e)$ is the pressure, $E=\rho(e+1/2u^2)$ is the total energy and the function $A(x)$ is the cross-sectional area of the duct at x. Specifically, as $A(x)=1$, the system (1.1) represents the planar compressible Euler equations.

In the development of numerical techniques approximating solutions of (1.1), the finite volume scheme plays an absolutely indispensable role, wherein one of the most crucial ingredients is the construction of numerical fluxes and it boils down to the resolution of associated (generalized) Riemann problems at each computational cell interface. Specifically, we denote by $I_j=[x_{j-1/2},x_{j+1/2}]$, $\Delta x=x_{j+1/2}-x_{j-1/2}$, the computational cell numbered j, and by $\{t_n\}_{n=0}^{\infty}$ the sequence of discretized time levels, $\Delta t=t_{n+1}-t_n$. The finite volume scheme is then constructed by integrating the governing equations (1.1) both in space and time over the control volume $I_j\times[t_{n+1},t_n)$ (see Fig. 1.1), yielding a "quasi-conservative" scheme

$$U_j^{n+1}=U_j^n-\frac{\Delta t}{(\Delta v)_j}\big[A(x_{j+1/2})F_{j+1/2}^{n+1/2}-A(x_{j-1/2})F_{j-1/2}^{n+1/2}\big]+\frac{\Delta t}{\Delta x}\big[G_{j+1/2}^{n+1/2}-G_{j-1/2}^{n+1/2}\big], \tag{1.2}$$

where

$$U_j^n=\frac{1}{\Delta x}\int_{x_{j-1/2}}^{x_{j+1/2}}U(x,t_n)\,\mathrm{d}x\quad\text{and}\quad(\Delta v)_j=\int_{x_{j-1/2}}^{x_{j+1/2}}A(x)\,\mathrm{d}x$$

are the average of $U(x,t^n)$ and the volume of the duct segment over cell I_j, respectively. The terms $F_{j+1/2}^{n+1/2}$ and $G_{j+1/2}^{n+1/2}$ in (1.2) are, respectively, the temporal average of $F(U(x,t))$ and $G(U(x,t))$ along the interface $x=x_{j+1/2}$, i.e.,

$$\begin{aligned}F_{j+1/2}^{n+1/2}&=\frac{1}{\Delta t}\int_{t_n}^{t_{n+1}}F\big(U(x_{j+\frac12},t)\big)\,\mathrm{d}t,\\ G_{j+1/2}^{n+1/2}&=\frac{1}{\Delta t}\int_{t_n}^{t_{n+1}}G\big(U(x_{j+\frac12},t)\big)\,\mathrm{d}t.\end{aligned} \tag{1.3}$$

For the notable Godunov scheme [10] and higher order schemes using Riemann solvers such as MUSCL [24,25] and TVD [11] schemes, in order to approximate $F_{j+1/2}^{n+1/2}$ and $G_{j+1/2}^{n+1/2}$ numerically, a classical Riemann problem is solved in each cell interface to evolve the solution from t^n to t^{n+1}. The corresponding initial data are taken as the interface limit values of $U(x,t^n)$ in the neighboring cells. As an extension, the GRP scheme assumes the piecewise smooth initial data and evolves solutions by analytically solving the generalized Riemann problem at each cell interface with at least second order accuracy. Currently, the second-order GRP scheme has already been exploited and put into use for several compressible fluid models [2,3,1,4,6,5,14,27,28]. Let us now outline a standard process for its implementation. Assume the data at time $t=t^n$ is piecewise linear with slope σ_j^n. That is, we have

$$U\big(x,t^n\big)=U_j^n+\sigma_j^n(x-x_j),\quad x\in I_j:=(x_{j-1/2},x_{j+1/2}). \tag{1.4}$$

Then the Godunov-type scheme of second order takes the form

$$U_j^{n+1} = U_j^n - \frac{\Delta t}{(\Delta v)_j}\big[A(x_{j+1/2})F_{j+1/2}^{n+1/2} - A(x_{j-1/2})F_{j-1/2}^{n+1/2}\big] + \frac{\Delta t}{\Delta x}\big[G_{j+1/2}^{n+1/2} - G_{j-1/2}^{n+1/2}\big], \tag{1.5}$$

where the following notations are used

$$F_{j+1/2}^{n+1/2} = F\big(U_{j+1/2}^{n+1/2}\big), \qquad G_{j+1/2}^{n+1/2} = G\big(U_{j+1/2}^{n+1/2}\big), \tag{1.6}$$

and $U_{j+1/2}^{n+1/2}$ is the mid-point value or the average of $U(x_{j+1/2}, t)$ over time interval $[t_n, t_{n+1}]$. The central issue is how to obtain the mid-point value $U_{j+1/2}^{n+1/2}$, which is formally approximated by the Taylor expansion (ignoring higher order terms)

$$U_{j+1/2}^{n+1/2} \cong U_{j+1/2}^n + \frac{\Delta t}{2}\left(\frac{\partial U}{\partial t}\right)_{j+1/2}^n, \tag{1.7}$$

where

$$U_{j+1/2}^n = \lim_{t\to t_n+0} U(x_{j+1/2}, t), \qquad \left(\frac{\partial U}{\partial t}\right)_{j+1/2}^n = \lim_{t\to t_n+0} \frac{\partial U}{\partial t}(x_{j+1/2}, t). \tag{1.8}$$

The value $U_{j+1/2}^n$ is obtained by solving the associated Riemann problem for the homogeneous hyperbolic conservation laws as used in the (first-order) Godunov scheme [10]. The main ingredient lies upon the calculation of the *instantaneous time derivative* $(\frac{\partial U}{\partial t})_{j+1/2}^n$.

For the solution U being smooth near the grid point $(x_{j+1/2}, t_n)$, it follows directly from (1.1) that

$$\left(\frac{\partial U}{\partial t}\right)_{j+1/2}^n = -\left[\frac{\partial F}{\partial U}\big(U_{j+1/2}^n\big) + \frac{\partial G}{\partial U}\big(U_{j+1/2}^n\big)\right]\left(\frac{\partial U}{\partial x}\right)_{j+1/2}^n - F\big(U_{j+1/2}^n\big)\frac{A'(x_{j+1/2})}{A(x_{j+1/2})}. \tag{1.9}$$

However, for the generalized Riemann problem including singularity at grid point $(x_{j+1/2}, t_n)$, (1.9) is no longer valid since there exist nonlinear waves (rarefaction waves or discontinuities) issuing from the singularity point $(x_{j+1/2}, t_n)$. Indeed, thinking of the initial data (1.4) with non-zero slopes as a perturbation of piecewise constant Riemann initial data and (1.1) as a perturbation of the homogeneous system of equations, the GRP solution is a perturbation of that of the *associated Riemann problem* at least in the neighborhood of the singularity point. It turns out that the GRP solution consists of, for a short time following the "disintegration" of initial discontinuity, the curved rarefaction wave and the discontinuities (contact discontinuity or shock wave) with time varying speed [4, Chap. 5].

The solution U together with its derivatives may undergo a jump discontinuity across each wave. Hence, in order to solve the generalized Riemann problem, it requires one to explore the mode of the discontinuity for the derivatives coming along with each wave, which is in fact described by a set of linear algebraic equations. This bears an analogy to the resolution of classical Riemann problem, which involves exploring the relation, usually described by a one parameter curve, between the two states of U connected by each wave. Indeed, the treatment for capturing the discontinuities of derivatives across each type of waves can be sketched out as follows.

A Since the generalized Riemann invariants (GRI) are transported in the transversal direction of the rarefaction fan, it is natural to use them for studying the variation of the derivatives across a rarefaction wave. Actually, the directional (emanating characteristic direction) derivatives of the GRI are determined by their values on either side of the wave.
B The GRI, which remain continuous across corresponding contact discontinuities, are differentiated in the direction of the discontinuity (characteristic).
C For the shock waves, the identities implied by the Rankine–Hugoniot conditions are differentiated along the shock trajectories.

As indicated in the previous works, the most technical step is the treatment of rarefaction fans, which relies on the analysis in term of "characteristic coordinates".

The methodology for resolving the generalized Riemann problem is originated in [2,3,1], wherein the original GRP is designed for the compressible fluid flows with two related Lagrangian and Eulerian versions. See also the recent textbook [4] for detailed discussions. The Eulerian version is always derived by using the Lagrangian case. The transformation is quite delicate, particularly for sonic cases, because it becomes singular at sonic points. The direct Eulerian version, more flexible for applications, is developed recently in the context of shallow water equations [14] and the compressible fluid flows [6,5]. The approach for solving GRP therein, being ready to handle any strict hyperbolic system endowed with a coordinate system of Riemann invariants (in particular, the two equations system), is extended to handle more general weakly coupled systems (in the sense of [5, Def. 21]) having only a "partial set" of Riemann invariants. However, the existing methods for deriving a second-order GRP solver are rather complicated, which prevents it from practical use in many ways. For example, the treatment of rarefaction relies heavily on the explicit formulation of the *Asymptotic Characteristic Coordinate* (ACC), which depends on the EOS (equation of state) of the fluid in turn and is sometimes hard to derive. Besides, the ACC is not easy to be written out explicitly for higher order GRP solvers that are particularly useful in capturing the propagation of entropy

wave [20] (see also Fig. 8.4). Other closely related efforts can be found in [7,13] using the approach of asymptotic analysis for the resolution of generalized Riemann problems, and in [12,23,8] (and the references therein) for approximate Godunov-type high order solvers. The solvers in [23,8] correspond to the acoustic case and they fail for resolving strong discontinuities (this point is confirmed through a numerical experiment, Fig. 7.2). Hence it is absolutely necessary to develop the high order (at least third order) GRP scheme by resolving nonlinear wave patterns at each computational grid point analytically, in addition to provide an acoustic approximation as the jump there is weak. Indeed, solvers of order higher than two is very few to be known besides a Navier–Stokes solver based on gas-kinetic formulation [16].

Therefore we present a new approach in this paper, still Eulerian, to resolve the GRP solvers for system (1.1). The solvers of second order as well as third order accuracy are derived. The resolution of rarefaction wave is simplified by using the new trick to derive the linear ODE systems for both second and third-order characteristic derivatives of GRI in the x–t coordinates without using the explicit formulation of ACC. Combining with the resolution of the contact discontinuity and the shock wave, the spatial derivatives of the solution in intermediate regions of the three waves are obtained by solving a simple system of linear algebraic equations. The case of sonic point is handled by calculating the derivatives of GRI and using the differential relation along the emanating characteristic curve. A special case frequently occurs during the numerical application of the GRP scheme is the acoustic case: the initial values of U are continuous but the derivatives are discontinuous at the singularity point. This case is comparatively easy to handle and requires less computation cost.

Although this paper focus on exploring solvers for the second-order *linear GRP* and the third-order *quadratic GRP*, higher order GRP solvers can be derived with the same methodology and a multidimensional extension can be pursued in a forthcoming work [15]. The resulting GRP solvers consist of two steps: (i) the classical Riemann solver; (ii) calculation of instantaneous time derivatives of U. As indicated by the solvers, step (ii) can be straightforward once the full Riemann solution is obtained. Besides, in both steps, only the limiting values of U and its spatial derivatives at two side of the singularity are used, and the resulting linear (resp. quadratic) GRP solver leads to second (resp. third) order accuracy in time approximation to U regardless its initial distribution.

This paper is arranged as follows. In Section 2, we introduce some preliminaries and notations, including some basic properties of the flow system and the basic setup for the GRP. The resolution of rarefaction waves and discontinuity waves, including the contact discontinuity and the shock wave, are detailed in Sections 3 and 4, respectively. We conclude the resolution of GRP in Section 5 and the acoustic approximation in Section 6. As an application example, we show the accuracy of the solvers by several tests in Section 7. Finally, in Section 8, the GRP solvers are used to construct one-step high order numerical schemes and a few 1-D numerical test cases are presented.

2. Preliminaries and notations

In this section we present some preliminaries for the resolution of generalized Riemann problems and some notations to be used.

Throughout this paper, the function $A(x)$ in (1.1) is assumed to be smooth or, to make precise, second-order continuously differentiable. Under this assumption, system (1.1) can be written in a conservative form as

$$\frac{\partial}{\partial t}U+\frac{\partial}{\partial x}F^{total}(U)=-\frac{A'(x)}{A(x)}F(U), \tag{2.1}$$

where $F^{total}(U)=F(U)+G(U)$.

Denoting by $Q:=(\rho,u,p)$ the vector of primitive variables, Eq. (2.1) takes the following nonconservative form equivalently in smooth flow regions

$$\frac{\partial}{\partial t}Q+J\frac{\partial}{\partial x}Q=H,\qquad J=\begin{pmatrix}u & \rho & 0\\ 0 & u & \frac{1}{\rho}\\ 0 & \rho c^2 & u\end{pmatrix},\qquad H=\begin{pmatrix}-\frac{A'(x)}{A(x)}\rho u\\ 0\\ -\frac{A'(x)}{A(x)}\rho c^2 u\end{pmatrix}, \tag{2.2}$$

where c is the local sound speed defined as $c^2=\frac{\partial p}{\partial\rho}(\rho,S)$. Here S stands for the specific entropy, and is related to other thermodynamical variables through the thermodynamic relation

$$T\,\mathrm{d}S=\mathrm{d}e-p\,\mathrm{d}\left(\frac{1}{\rho}\right).$$

The system (2.1) or (2.2) possesses three eigenvalues

$$\lambda_-=u-c,\qquad \lambda_0=u,\qquad \lambda_+=u+c.$$

Associated with λ_-, λ_0, λ_+, the three pairs

$$\boldsymbol{w}_-=(S,\psi_-),\qquad \boldsymbol{w}_0=(u,p),\qquad \boldsymbol{w}_+=(S,\psi_+)$$

are the *generalized Riemann invariants* (*GRI*), respectively, where the two variables ψ_- and ψ_+ are defined by

$$\psi_{\mp} = u \pm \int^{\rho} \frac{c(\omega, S)}{\omega}\, \mathrm{d}\omega.$$

Corresponding to the three characteristic fields, we have the following set of equations describing the differential relations along each characteristic curve

$$\begin{cases} \dfrac{Dp}{Dt} - c^2 \dfrac{D\rho}{Dt} = 0, \\ \dfrac{D_{\pm}u}{Dt} \pm \dfrac{1}{\rho c} \dfrac{D_{\pm}p}{Dt} = \mp \dfrac{A'}{A} uc, \end{cases} \tag{2.3}$$

where the differential operators

$$\frac{D}{Dt} := \frac{\partial}{\partial t} + u \frac{\partial}{\partial x} \quad \text{and} \quad \frac{D_{\pm}}{Dt} := \frac{\partial}{\partial t} + \lambda_{\pm} \frac{\partial}{\partial x}$$

denote the total derivative operators along the characteristic curves: $x'(t) = u$ and $x'(t) = u \pm c$, respectively.

The first equation of (2.3) is equivalent to the invariance of the entropy S along the λ_0-characteristic curve, i.e.,

$$\frac{DS}{Dt} = 0. \tag{2.4}$$

Introduce the new variable

$$K(\rho, S) = -\frac{1}{\rho c} \frac{\partial p}{\partial S} + \frac{\partial \psi_-}{\partial S} \tag{2.5}$$

and note that $\frac{\partial \psi_-}{\partial S} = -\frac{\partial \psi_+}{\partial S}$. Then in terms of total differentials we have

$$\mathrm{d}\psi_{\mp} \mp K(\rho, S)\, \mathrm{d}S = \mathrm{d}u \pm \frac{1}{\rho c}\, \mathrm{d}p. \tag{2.6}$$

Hence, from the relations between $\frac{D_{\mp}u}{Dt}$ and $\frac{D_{\mp}p}{Dt}$ in (2.3), we get

$$\frac{D_{\pm}\psi_{\mp}}{Dt} \mp K(\rho, S) \frac{D_{\pm}S}{Dt} = \mp \frac{A'}{A} uc. \tag{2.7}$$

In particular, for the important case of polytropic gases, the thermal equation of state is given by

$$p = (\gamma - 1)\rho e, \quad \gamma > 1, \tag{2.8}$$

and the two variables $\psi_{\mp}$ are

$$\psi_{\mp} = u \pm \frac{2c}{\gamma - 1},$$

where $c^2 = \frac{\gamma p}{\rho}$. It follows that

$$2c \frac{\partial c}{\partial S} = \frac{\gamma}{\rho} \frac{\partial p}{\partial S} \quad \text{and} \quad \frac{\partial \psi_-}{\partial S} = \frac{2}{\gamma - 1} \frac{\partial c}{\partial S} = \frac{\gamma}{(\gamma - 1)\rho c} \frac{\partial p}{\partial S}.$$

Also note that, for this case,

$$T\, \mathrm{d}S = \frac{\mathrm{d}p}{(\gamma - 1)\rho} - \frac{c^2}{(\gamma - 1)\rho}\, \mathrm{d}\rho. \tag{2.9}$$

Hence, from (2.5) we obtain

$$K(\rho, S) = \frac{1}{(\gamma - 1)\rho c} \frac{\partial p}{\partial S} = \frac{T}{c}.$$

Now let us introduce the generalized Riemann problem. It is defined as the initial-value problem for system (2.1), subject to the initial data

$$U(x, 0) = \begin{cases} P_-(x) & \text{if } x < 0, \\ P_+(x) & \text{if } x > 0, \end{cases} \tag{2.10}$$

where $P_{\pm}(x)$ are vectors, whose components are the smooth functions. As illustrated in Section 1, the initial structure of the solution is determined by the *associated Riemann problem*:

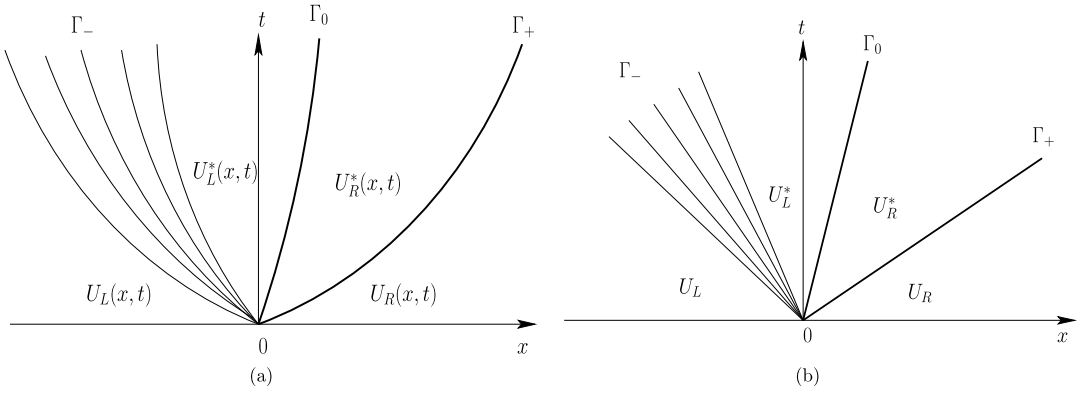

Fig. 2.1. The schematic description of the local wave configurations: (a) Wave patterns for the GRP with initial data $U(0,x) = P_-(x)$ for $x < 0$ and $U(0,x) = P_+(x)$ for $x > 0$. (b) Wave patterns for the associated Riemann problem.

$$\begin{cases} \dfrac{\partial}{\partial t}U^A + \dfrac{\partial}{\partial x}F^{total}\big(U^A\big) = 0, \\ U^A(x,0) = U_\pm, \quad \pm x > 0, \end{cases} \tag{2.11}$$

where $U_\pm$ are the limiting values of $P_\pm(x)$ at $x = 0$, i.e., $U_\pm = P_\pm(0^\pm)$. We call the solution of (2.11) the *associated Riemann solution* of (2.1) and (2.10).

Denote by $R^A(x/t, U_-, U_+)$ the Riemann solution of (2.11). Then we have the following proposition.

Proposition 2.1. *Let $U(x,t)$ be the solution to the generalized Riemann problem (2.1) and (2.10). Then for every fixed direction $\theta = x/t$,*

$$\lim_{t\to 0} U(\theta t, t) = R^A(\theta, U_-, U_+). \tag{2.12}$$

This implies that the local wave configuration for the generalized Riemann problem (2.1) and (2.10) is identical, near the singularity at $(x,t) = (0,0)$, to that of the associated Riemann problem (2.11).

Proposition 2.1 is illustrated schematically in Fig. 2.1. The solution of (2.11) is self-similar, and hence the waves are centered. Correspondingly, the waves for (2.1) are curved (see [4] for more detailed descriptions).

We emphasize that the solution U is smooth in the intermediate regions of these waves and along each emanating characteristic curve in the rarefaction fan (up to the singularity $(0,0)$). To approximate U along t-axis with kth order accuracy, we can use the Taylor expansion

$$U(x=0,t) = U(0,0) + \sum_{\ell=1}^{k} \frac{1}{\ell!}\frac{\partial^\ell U}{\partial t^\ell}(0,0)\cdot t^k + \mathcal{O}\big(t^{k+1}\big). \tag{2.13}$$

A solver of the GRP is actually that of evaluating the instantaneous time derivatives

$$\frac{\partial^\ell U}{\partial t^\ell}(0,0) = \lim_{t\to 0}\frac{\partial^\ell U}{\partial t^\ell}(0,t), \quad t > 0. \tag{2.14}$$

For convenience, we label the problem of evaluating (2.14) with $\ell = 1$ (resp. $\ell = 1, 2$) as the *linear GRP* (resp. *quadratic GRP*), or *LGRP* (reps. *QGRP*) for short. As mentioned in the introduction, this paper concentrates on QGRP.

Although there are other local wave configurations, we will restrict our discussion to the local wave configuration shown in Fig. 2.1, where a rarefaction wave moves to the left, a shock moves to the right. The intermediate region is separated by a contact discontinuity. Other local wave configurations may be similarly considered and will be briefly discussed. Finally, we make a rule for the notations as follows. For any variable V including the state variable U and their derivatives, we shall denote respectively by V_L and V_R the limiting values of V as $t \to 0^+$ in the two subregions adjacent to x-axis, and respectively by V_L^* and V_R^* the limiting values of V as $t \to 0^+$ in the two intermediate subregions. Besides, the limiting state of V at $x = 0$ as $t \to 0^+$ will be denoted by V_*.

3. Resolution of curved rarefaction waves

This section gives the resolution of left rarefaction wave Γ_- associated with λ_- for the GRP (2.1) and (2.10). As pointed out earlier, this is the main step of the GRP methodology and the main ingredients are the resolution of generalized Riemann invariants.

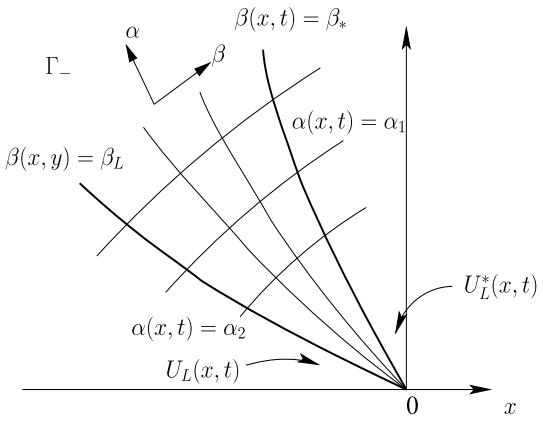

Fig. 3.1. The characteristic coordinates for the rarefaction wave Γ_-.

Actually, the rarefaction wave Γ_- will be resolved by using Eqs. (2.4) and (2.7) for S and ψ_- to track the directional derivatives of GRI $\frac{D_-^\ell S}{Dt^\ell}$ and $\frac{D_-^\ell \psi_-}{Dt^\ell}$ $(\ell=1,2)$ in the rarefaction fan, respectively. However, we cannot apply the operators $\frac{D_-^\ell}{Dt^\ell}$ to (2.4) or (2.7) directly since the directional derivatives $\frac{D_-}{Dt}$ and $\frac{D}{Dt}$ (or $\frac{D_+}{Dt}$) are not commutable. Hence we need to use the characteristic coordinates, which work similarly to the usual polar coordinates to single out the singularity of a rarefaction fan. For simplicity of notations, in the remainder of this section we shall write λ, $\boldsymbol{w}$ and ψ for λ_-, $\boldsymbol{w}_-$ and ψ_-, respectively, by suppressing the subscript.

The region of rarefaction wave Γ_- is described by the set $\mathcal{R}=\{(\alpha(x,y),\beta(x,y)) \mid 0\leqslant\alpha<+\infty,\beta\in[\beta_L,\beta_*]\}$, where $\beta_L=\lambda(U_L)$, $\beta_*=\lambda(U_L^*)$, and $\beta(x,t)=\beta$ and $\alpha(x,t)=\alpha$ are the integral curves of the following equations, respectively,

$$\frac{\mathrm{d}x}{\mathrm{d}t}=\lambda,\qquad \frac{\mathrm{d}x}{\mathrm{d}t}=\mu, \tag{3.1}$$

where μ is the slope of a family of transversal curves and it bears multiple choices. For example, it can be taken as λ_0, λ_+ or $-t/x$. Moreover, β and α are denoted as follows: β is the initial value of the slope λ at the singularity $(x,t)=(0,0)$ and α is the t-coordinate of the intersection point of a transversal curve with the leading β-curve: $\beta=\beta_L$.

The coordinates (x,t) in the "triangle" sector of Γ_- shown in Fig. 3.1 can be expressed in terms of α and β,

$$x=x(\alpha,\beta),\qquad t=t(\alpha,\beta), \tag{3.2}$$

which satisfy

$$\frac{\partial x}{\partial\alpha}=\lambda\frac{\partial t}{\partial\alpha},\qquad \frac{\partial x}{\partial\beta}=\mu\frac{\partial t}{\partial\beta}. \tag{3.3}$$

In the following, we shall call (α,β) the *characteristic coordinates* associated with λ and λ_0 (resp. λ_+) if $\mu=\lambda_0$ (resp. $\mu=\lambda_+$).

Denote $\frac{D_\mu}{Dt}:=\frac{\partial}{\partial t}+\mu\frac{\partial}{\partial x}$ and recall the definition of $\frac{D_-}{Dt}$. Then we have

$$\frac{\partial}{\partial\alpha}=\frac{\partial t}{\partial\alpha}\frac{D_-}{Dt},\qquad \frac{\partial}{\partial\beta}=\frac{\partial t}{\partial\beta}\frac{D_\mu}{Dt}. \tag{3.4}$$

Moreover, we have at $\alpha=0$,

$$\frac{\partial\lambda}{\partial\beta}(0,\beta)=1,\qquad \frac{\partial t}{\partial\beta}(0,\beta)=0,\quad \beta\in[\beta_L,\beta_*]. \tag{3.5}$$

By differentiating the first equation in (3.3) with respect to β, the second with respect to α and then subtracting, we find that the function $t=t(\alpha,\beta)$ satisfies

$$(\mu-\lambda)\frac{\partial^2 t}{\partial\alpha\partial\beta}=\frac{\partial\lambda}{\partial\beta}\frac{\partial t}{\partial\alpha}-\frac{\partial\mu}{\partial\alpha}\frac{\partial t}{\partial\beta}. \tag{3.6}$$

Setting $\alpha=0$ and using (3.5), one obtains

$$\frac{\partial}{\partial\beta}\left[\frac{\partial t}{\partial\alpha}(0,\beta)\right]=\frac{1}{\mu-\lambda}\frac{\partial t}{\partial\alpha}(0,\beta). \tag{3.7}$$

We continue to make differentiation of (3.6) with respect to α to get

$$(\mu-\lambda)\frac{\partial^3 t}{\partial\alpha^2\partial\beta}=-\frac{\partial}{\partial\alpha}(\mu-\lambda)\frac{\partial^2 t}{\partial\alpha\partial\beta}+\frac{\partial^2\lambda}{\partial\alpha\partial\beta}\frac{\partial t}{\partial\alpha}+\frac{\partial\lambda}{\partial\beta}\frac{\partial^2 t}{\partial\alpha^2}-\frac{\partial^2\mu}{\partial\alpha^2}\frac{\partial t}{\partial\beta}-\frac{\partial\mu}{\partial\alpha}\frac{\partial^2 t}{\partial\alpha\partial\beta}. \tag{3.8}$$

Recalling (3.5) and (3.7) as well as noticing

$$\frac{\partial^2}{\partial\alpha\partial\beta}\lambda=\frac{\partial}{\partial\beta}\left(\frac{\partial t}{\partial\alpha}\frac{D_-\lambda}{Dt}\right)=\frac{\partial^2 t}{\partial\alpha\partial\beta}\frac{D_-\lambda}{Dt}+\frac{\partial t}{\partial\alpha}\frac{\partial}{\partial\beta}\left(\frac{D_-\lambda}{Dt}\right),$$

we can obtain, by setting $\alpha=0$ in (3.8),

$$\begin{aligned}\frac{\partial}{\partial\beta}\left[\frac{\partial^2 t}{\partial\alpha^2}(0,\beta)\right]&=\frac{1}{\mu-\lambda}\frac{\partial^2 t}{\partial\alpha^2}(0,\beta)+\frac{D_-}{Dt}\left(\frac{2}{\mu-\lambda}\right)\left(\frac{\partial t}{\partial\alpha}\right)^2(0,\beta)\\&\quad+\frac{1}{\mu-\lambda}\frac{\partial}{\partial\beta}\left(\frac{D_-\lambda}{Dt}\right)\left(\frac{\partial t}{\partial\alpha}\right)^2(0,\beta).\end{aligned} \tag{3.9}$$

With the aid of Eqs. (3.7) and (3.9), we obtain the following lemma regarding expressions of the operators $\frac{\partial^{\ell+1}}{\partial\beta\partial\alpha^\ell}$, $\ell=1,2$, at $\alpha=0$.

Lemma 3.1. *For $\alpha=0$ and $\beta\in[\beta_L,\beta_*]$, the operators $\frac{\partial^2}{\partial\beta\partial\alpha}$ and $\frac{\partial^3}{\partial\beta\partial\alpha^2}$ can be expressed as*

$$\frac{\partial^2}{\partial\beta\partial\alpha}=\frac{\partial t}{\partial\alpha}\mathcal{D}^{(1)}_{\lambda,\mu}, \tag{3.10}$$

and

$$\frac{\partial^3}{\partial\beta\partial\alpha^2}=\left(\frac{\partial t}{\partial\alpha}\right)^2\mathcal{D}^{(2)}_{\lambda,\mu}+\frac{\partial^2 t}{\partial\alpha^2}\mathcal{D}^{(1)}_{\lambda,\mu}, \tag{3.11}$$

respectively, where the operators $\mathcal{D}^{\ell}_{\lambda,\mu}$, for $\ell=1,2$, are defined as

$$\mathcal{D}^{(1)}_{\lambda,\mu}:=\frac{\partial}{\partial\beta}\left(\frac{D_-}{Dt}\cdot\right)+\frac{1}{\mu-\lambda}\frac{D_-}{Dt}, \tag{3.12}$$

and

$$\mathcal{D}^{(2)}_{\lambda,\mu}:=\frac{\partial}{\partial\beta}\left(\frac{D_-^2}{Dt^2}\cdot\right)+\frac{2}{\mu-\lambda}\frac{D_-^2}{Dt^2}+\left[\frac{D_-}{Dt}\left(\frac{2}{\mu-\lambda}\right)+\frac{1}{\mu-\lambda}\frac{\partial}{\partial\beta}\left(\frac{D_-\lambda}{Dt}\right)\right]\frac{D_-}{Dt}, \tag{3.13}$$

respectively.

Proof. Using the chain rule, we have

$$\frac{\partial^2}{\partial\beta\partial\alpha}=\frac{\partial}{\partial\beta}\left(\frac{\partial t}{\partial\alpha}\frac{D_-}{Dt}\cdot\right)=\frac{\partial t}{\partial\alpha}\frac{\partial}{\partial\beta}\left(\frac{D_-}{Dt}\cdot\right)+\frac{\partial^2 t}{\partial\beta\partial\alpha}\frac{D_-}{Dt}, \tag{3.14}$$

and

$$\begin{aligned}\frac{\partial^3}{\partial\beta\partial\alpha^2}&=\frac{\partial}{\partial\beta}\left(\frac{\partial}{\partial\alpha}\left(\frac{\partial t}{\partial\beta}\frac{D_-}{Dt}\cdot\right)\right)=\frac{\partial}{\partial\beta}\left[\frac{\partial^2 t}{\partial\alpha^2}\frac{D_-}{Dt}+\left(\frac{\partial t}{\partial\alpha}\right)^2\frac{D_-^2}{Dt^2}\right]\\&=\left(\frac{\partial t}{\partial\alpha}\right)^2\frac{\partial}{\partial\beta}\left(\frac{D_-^2}{Dt^2}\cdot\right)+2\frac{\partial^2 t}{\partial\beta\partial\alpha}\frac{\partial t}{\partial\alpha}\frac{D_-^2}{Dt^2}+\frac{\partial^2 t}{\partial\alpha^2}\frac{\partial}{\partial\beta}\left(\frac{D_-}{Dt}\cdot\right)+\frac{\partial^3 t}{\partial\beta\partial\alpha^2}\frac{D_-}{Dt}.\end{aligned} \tag{3.15}$$

Then we can obtain (3.10) and (3.11) at $\alpha=0$ by inserting (3.7) and (3.9) into (3.14) and (3.15). □

Our main result about the generalized Riemann invariant $\boldsymbol{w}=(S,\psi)$ is that, at $\alpha=0$, the *characteristic derivative* $\frac{D_-\boldsymbol{w}}{Dt}(0,\beta)$ (resp. $\frac{D_-^2\boldsymbol{w}}{Dt^2}(0,\beta)$) is continuously differentiable as a function of β and satisfies a set of linear ordinary differential equations, referred to as the *linear* (*resp. quadratic*) *GRP equations*, which is precisely stated in the following lemma.

Lemma 3.2 *(Linear and quadratic GRP equations of GRI). In the region of left rarefaction wave Γ_-, we have the following set of linear GRP equations for S and ψ:*

$$\begin{cases} \dfrac{\partial}{\partial\beta}\left[\dfrac{D_-S}{Dt}(0,\beta)\right] = -\dfrac{1}{c}\dfrac{D_-S}{Dt}, \\ \dfrac{\partial}{\partial\beta}\left[\dfrac{D_-\psi}{Dt}(0,\beta)\right] = -\dfrac{1}{2c}\dfrac{D_-\psi}{Dt} - \dfrac{K}{2c}\dfrac{D_-S}{Dt} - \dfrac{A'}{2A}u, \end{cases} \tag{3.16}$$

and quadratic GRP equations:

$$\begin{cases} \dfrac{\partial}{\partial\beta}\left[\dfrac{D_-^2S}{Dt^2}(0,\beta)\right] = -\dfrac{2}{c}\dfrac{D_-^2S}{Dt^2} - \left[\dfrac{D_-}{Dt}\left(\dfrac{2}{c}\right) + \dfrac{1}{c}\dfrac{\partial}{\partial\beta}\left(\dfrac{D_-\lambda}{Dt}\right)\right]\dfrac{D_-S}{Dt}, \\ \dfrac{\partial}{\partial\beta}\left[\dfrac{D_-^2\psi}{Dt^2}(0,\beta)\right] = -\dfrac{1}{c}\dfrac{D_-^2\psi}{Dt^2} - \dfrac{K}{c}\dfrac{D_-^2S}{Dt^2} \\ \qquad\qquad - \left[\dfrac{D_-}{Dt}\left(\dfrac{1}{c}\right) + \dfrac{1}{2c}\dfrac{\partial}{\partial\beta}\left(\dfrac{D_-\lambda}{Dt}\right)\right]\left(\dfrac{D_-\psi}{Dt} + K\dfrac{D_-S}{Dt}\right) \\ \qquad\qquad - \dfrac{1}{c}\dfrac{D_-K}{Dt}\dfrac{D_-S}{Dt} - \dfrac{A'}{2A}u\dfrac{\partial}{\partial\beta}\left(\dfrac{D_-\lambda}{Dt}\right) - \dfrac{D_-}{Dt}\left(\dfrac{A'}{A}u\right), \end{cases} \tag{3.17}$$

for $\beta \in [\beta_L, \beta_*]$.

Remark 3.1. (i) By noticing that

$$\begin{cases} \dfrac{\partial S}{\partial x} = -\dfrac{1}{c}\dfrac{D_-S}{Dt}, \\ \dfrac{\partial\psi}{\partial x} = -\dfrac{1}{2c}\left(\dfrac{D_-\psi}{Dt} + K\dfrac{D_-S}{Dt}\right) - \dfrac{A'}{2A}u, \end{cases}$$

we see that $\frac{\partial \boldsymbol{w}}{\partial x}$ takes finite value at $\alpha = 0$, which remains continuous across both the head β-curve: $\beta = \beta_L$ and the tail β-curve: $\beta = \beta_*$, as $\frac{D_-\boldsymbol{w}}{Dt}(0,\beta)$ does. Moreover, (3.16) is equivalent to the following set of equations for $\frac{\partial S}{\partial x}$ and $\frac{\partial\psi}{\partial x}$:

$$\begin{cases} \dfrac{\partial}{\partial\beta}\left[\dfrac{\partial S}{\partial x}(0,\beta)\right] = -\dfrac{1}{c}\left(1 + \dfrac{\partial c}{\partial\beta}\right)\dfrac{\partial S}{\partial x}, \\ \dfrac{\partial}{\partial\beta}\left[\dfrac{\partial\psi}{\partial x}(0,\beta)\right] = -\dfrac{1}{c}\left(\dfrac{1}{2} + \dfrac{\partial c}{\partial\beta}\right)\dfrac{\partial\psi}{\partial x} + \dfrac{1}{2}\left(\dfrac{\partial K}{\partial\beta} - \dfrac{K}{c}\right)\dfrac{\partial S}{\partial x} - \dfrac{1}{2c}\dfrac{\partial}{\partial\beta}\left(\dfrac{A'}{A}uc\right), \end{cases} \tag{3.18}$$

for $\beta \in [\beta_L, \beta_*]$. However, the second-order derivative $\frac{\partial^2\boldsymbol{w}}{\partial x^2}(0,\beta)$ does not take a finite value in general for $\beta \in (\beta_L, \beta_*)$.

(ii) From the second equation of (2.7), we can get

$$\begin{aligned} &\frac{D_-\psi_+}{Dt}(0,\beta) = \left[-K\frac{D_-S}{Dt} + \frac{A'}{A}uc\right], \\ &\frac{D_-^2\psi_+}{Dt^2}(0,\beta) = -\left[K\frac{D_-^2S}{Dt^2} + \frac{D_-}{Dt}K\frac{D_-S}{Dt} + \frac{D_-}{Dt}\left(\frac{A'}{A}cu\right)\right]. \end{aligned} \tag{3.19}$$

Lemma 3.2 and Eq. (3.19) imply that $\frac{D_-^\ell U}{Dt^\ell}(0,\beta)$, for $\ell = 1, 2$, take finite values. This is consistent with our assumption of the GRP solution.

Proof of Lemma 3.2. Let (α, β) be the characteristic coordinates associated with λ and λ_0. Then, from (2.4), we have

$$\frac{\partial S}{\partial\beta} = \frac{\partial t}{\partial\beta}\frac{DS}{Dt} = 0 \tag{3.20}$$

and it follows that

$$\frac{\partial^{\ell+1}S}{\partial\beta\partial\alpha^\ell} = 0, \tag{3.21}$$

for $\ell = 1, 2$. At $\alpha = 0$, by expanding the operators $\frac{\partial^{\ell+1}}{\partial\beta\partial\alpha^\ell}$, $\ell = 1, 2$ in (3.21) using (3.10) and (3.11), we obtain

$$\mathcal{D}^{(\ell)}_{\lambda,\lambda_0}S = 0. \tag{3.22}$$

We refer to (3.12) and (3.13) for the notations $\mathcal{D}^{(\ell)}_{\lambda,\lambda_0}$, $\ell = 1, 2$.

Next, we shall use the characteristic coordinates associated with λ and λ_+, which is also denoted by (α,β). Multiplying $\frac{\partial t}{\partial\beta}$ to the first equation of (2.7) yields

$$\frac{\partial\psi}{\partial\beta}=K\frac{\partial S}{\partial\beta}-\frac{\partial t}{\partial\beta}\left(\frac{A'}{A}uc\right). \tag{3.23}$$

Then we differentiate (3.23) with respect to α to get

$$\frac{\partial^2\psi}{\partial\beta\partial\alpha}=K\frac{\partial^2 S}{\partial\beta\partial\alpha}+\frac{\partial K}{\partial\alpha}\frac{\partial S}{\partial\beta}-\frac{\partial^2 t}{\partial\beta\partial\alpha}\left(\frac{A'}{A}uc\right)-\frac{\partial t}{\partial\beta}\frac{\partial}{\partial\alpha}\left(\frac{A'}{A}uc\right). \tag{3.24}$$

Setting $\alpha=0$, inserting (3.7) into (3.24) and using (3.10) to expand $\frac{\partial^2\psi}{\partial\beta\partial\alpha}$ and $\frac{\partial^2 S}{\partial\beta\partial\alpha}$, we obtain

$$\mathcal{D}^{(1)}_{\lambda,\lambda_+}\psi=K\mathcal{D}^{(1)}_{\lambda,\lambda_+}S+\frac{1}{\lambda_+-\lambda}\left(\frac{A'}{A}uc\right), \tag{3.25}$$

where we have also used (3.5) and the fact that $\frac{\partial S}{\partial\beta}(0,\beta)=0$.

Differentiating (3.24) with respect to α once again yields

$$\begin{aligned}\frac{\partial^3\psi}{\partial\beta\partial\alpha^2}=&K\frac{\partial^3 S}{\partial\beta\partial\alpha^2}+2\frac{\partial K}{\partial\alpha}\frac{\partial^2 S}{\partial\alpha\partial\beta}+\frac{\partial^2 K}{\partial\alpha^2}\frac{\partial S}{\partial\beta}\\&-\frac{\partial^3 t}{\partial\beta\partial\alpha^2}\left(\frac{A'}{A}uc\right)-2\frac{\partial^2 t}{\partial\alpha\partial\beta}\frac{\partial}{\partial\alpha}\left(\frac{A'}{A}uc\right)-\frac{\partial t}{\partial\beta}\frac{\partial^2}{\partial\alpha^2}\left(\frac{A'}{A}uc\right).\end{aligned} \tag{3.26}$$

At $\alpha=0$, by inserting (3.7), (3.9) into (3.26) and using (3.10) and (3.11) to expand the operators $\frac{\partial^2}{\partial\beta\partial\alpha}$ and $\frac{\partial^3}{\partial\beta\partial\alpha^2}$ before ψ and S, respectively, we obtain

$$\begin{aligned}&\left(\frac{\partial t}{\partial\alpha}\right)^2\mathcal{D}^{(2)}_{\lambda,\lambda_+}\psi+\frac{\partial^2 t}{\partial\alpha^2}\mathcal{D}^{(1)}_{\lambda,\lambda_+}\psi=\left(\frac{\partial t}{\partial\alpha}\right)^2K\mathcal{D}^{(2)}_{\lambda,\lambda_+}S+\frac{\partial^2 t}{\partial\alpha^2}K\mathcal{D}^{(1)}_{\lambda,\lambda_+}S\\&+2\left(\frac{\partial t}{\partial\alpha}\right)^2\frac{D_-K}{Dt}\mathcal{D}^{(1)}_{\lambda,\lambda_+}S+\frac{2}{\lambda_+-\lambda}\left(\frac{\partial t}{\partial\alpha}\right)^2\frac{D_-}{Dt}\left(\frac{A'}{A}uc\right)\\&+\left[\frac{1}{\lambda_+-\lambda}\frac{\partial^2 t}{\partial\alpha^2}+\frac{D_-}{Dt}\left(\frac{2}{\lambda_+-\lambda}\right)\left(\frac{\partial t}{\partial\alpha}\right)^2+\frac{1}{\lambda_+-\lambda}\frac{\partial}{\partial\beta}\left(\frac{D_-\lambda}{Dt}\right)\left(\frac{\partial t}{\partial\alpha}\right)^2\right]\left(\frac{A'}{A}uc\right).\end{aligned} \tag{3.27}$$

With the aid of (3.25), (3.27) can be simplified as

$$\mathcal{D}^{(2)}_{\lambda,\lambda_+}\psi=K\mathcal{D}^{(2)}_{\lambda,\lambda_+}S+2\frac{D_-K}{Dt}\mathcal{D}^{(1)}_{\lambda,\lambda_+}S-\frac{A'}{2A}u\frac{\partial}{\partial\beta}\left(\frac{D_-\lambda}{Dt}\right)-\frac{D_-}{Dt}\left(\frac{A'}{A}u\right). \tag{3.28}$$

Note that

$$\begin{aligned}&\mathcal{D}^{(1)}_{\lambda,\lambda_+}S=\mathcal{D}^{(1)}_{\lambda,\lambda_0}S-\frac{1}{2c}\frac{D_-S}{Dt}=-\frac{1}{2c}\frac{D_-S}{Dt},\\&\mathcal{D}^{(2)}_{\lambda,\lambda_+}S=\mathcal{D}^{(2)}_{\lambda,\lambda_0}S-\mathcal{D}^{(2)}_{\lambda}S=-\mathcal{D}^{(2)}_{\lambda}S,\end{aligned}$$

and

$$\mathcal{D}^{(2)}_{\lambda,\lambda_+}\psi=\frac{\partial}{\partial\beta}\left(\frac{D_-^2\psi}{Dt^2}\right)^2+\mathcal{D}^{(2)}_{\lambda}\psi,$$

where

$$\mathcal{D}^{(2)}_{\lambda}:=\frac{1}{c}\frac{D_-^2}{Dt^2}+\left[\frac{D_-}{Dt}\left(\frac{1}{c}\right)+\frac{1}{2c}\frac{\partial}{\partial\beta}\left(\frac{D_-\lambda}{Dt}\right)\right]\frac{D_-}{Dt}.$$

From (3.28), it follows that

$$\frac{\partial}{\partial\beta}\left[\frac{D_-^2\psi}{Dt^2}(0,\beta)\right]=-\mathcal{D}^{(2)}_{\lambda}\psi-K\mathcal{D}^{(2)}_{\lambda}S-\frac{1}{c}\frac{D_-K}{Dt}\frac{D_-S}{Dt}-\frac{A'}{2A}u\frac{\partial}{\partial\beta}\left(\frac{D_-\lambda}{Dt}\right)-\frac{D_-}{Dt}\left(\frac{A'}{A}u\right). \tag{3.29}$$

Combining (3.22), (3.25) and (3.29), we finally obtain (3.16) and (3.17). □

For the polytropic cases, by recalling that $S(0,\beta)=S_L$, $\psi(0,\beta)=\psi_L$, $\lambda_-(0,\beta)=\beta$ in the rarefaction fan of Γ_-, $\frac{D_-\boldsymbol{w}}{Dt}(0,\beta)$ and $\frac{D_-^2\boldsymbol{w}}{Dt^2}(0,\beta)$ can be formulated by integrating (3.16) and (3.17), respectively.

Lemma 3.3 *(Derivatives of GRI for polytropic cases). For the polytropic cases with $\gamma > 1$, we have*

$$\begin{aligned}
&\frac{D_- S}{Dt}(0,\beta) = A_1(\psi_L-\beta)^{\frac{\gamma+1}{\gamma-1}},\\
&\frac{D_-\psi}{Dt}(0,\beta) = A_2(\psi_L-\beta)^{\frac{\gamma+1}{2(\gamma-1)}} + A_3(\psi_L-\beta)^{\frac{2\gamma}{\gamma-1}} + Z_0^\gamma(\beta)(\psi_L-\beta)^{\frac{\gamma+1}{2(\gamma-1)}},
\end{aligned} \tag{3.30}$$

and

$$\begin{aligned}
&\frac{D_-^2 S}{Dt}(0,\beta) = \left[(\psi_L-\beta_L)^{-\frac{2(\gamma+1)}{\gamma-1}}\frac{D_-^2 S}{Dt^2}(0,\beta_L) + Z_1^\gamma(\beta) - Z_1^\gamma(\beta_L)\right](\psi_L-\beta)^{\frac{2(\gamma+1)}{\gamma-1}},\\
&\frac{D_-^2\psi}{Dt^2}(0,\beta) = \left[(\psi_L-\beta_L)^{-\frac{\gamma+1}{\gamma-1}}\frac{D_-^2\psi}{Dt^2}(0,\beta_L) + Z_2^\gamma(\beta) - Z_2^\gamma(\beta_L)\right](\psi_L-\beta)^{\frac{\gamma+1}{\gamma-1}},
\end{aligned} \tag{3.31}$$

for $\beta\in[\beta_L,\beta_L^*]$, where

$$A_1 = (\psi_L-\beta_L)^{-\frac{\gamma+1}{\gamma-1}}\frac{D_- S}{Dt}(0,\beta_L), \qquad A_2 = \tilde{A}_2 - Z_0^\gamma(\beta_L),$$

and

$$\tilde{A}_2 = -A_3(\psi_L-\beta_L)^{\frac{3\gamma-1}{2(\gamma-1)}} + (\psi_L-\beta_L)^{-\frac{\gamma+1}{2(\gamma-1)}}\frac{D_-\psi}{Dt}(0,\beta_L),$$

$$Z_0^\gamma(\beta) = \begin{cases} B_1(\psi_L-\beta)^{\frac{\gamma-3}{2(\gamma-1)}} + B_2(\psi_L-\beta)^{\frac{3\gamma-5}{2(\gamma-1)}}, & \text{if } \gamma\neq 3,5/3;\\ \frac{\psi_L}{2}\frac{A'(x)}{A(x)}\ln(\psi_L-\beta) + B_2(\psi_L-\beta), & \text{if } \gamma = 3;\\ B_1(\psi_L-\beta)^{-\frac{7}{4}} - \frac{3}{8}\frac{A'(x)}{A(x)}\ln(\psi_L-\beta), & \text{if } \gamma = 5/3. \end{cases}$$

Moreover, the coefficients A_3, B_1, B_2, $Z_1^\gamma(\beta)$ and $Z_2^\gamma(\beta)$ will be given in Appendix A.

Remark 3.2. The derivatives of ψ_+, $\frac{D_-^\ell\psi_+}{Dt^\ell}(0,\beta)$ $(\ell=1,2)$, can be determined by (3.19). For example, for $\ell=1$, we have

$$\frac{D_-\psi_+}{Dt}(0,\beta) = A_4(\psi_L-\beta)^{\frac{2\gamma}{\gamma-1}} + B_3(\psi_L-\beta) + B_4(\psi_L-\beta)^2, \tag{3.32}$$

where the coefficients A_4, B_3, B_4 are also given in Appendix A.

Moreover, by noticing that $\lambda = \frac{3-\gamma}{4}\psi + \frac{1+\gamma}{4}\psi_+$ and $c = \frac{\gamma-1}{4}(\psi-\psi_L)$, $\frac{D_-^\ell\lambda}{Dt^\ell}(0,\beta)$ and $\frac{D_-^\ell c}{Dt^\ell}(0,\beta)$ $(\ell=1,2)$ can be obtained from (3.30), (3.31) and (3.32).

Lemma 3.4. *For $\ell=1,2$, the limiting values $(\frac{\partial^\ell u}{\partial x^\ell})_L^*$, $(\frac{\partial^\ell p}{\partial x^\ell})_L^*$ and $(\frac{\partial^\ell \rho}{\partial x^\ell})_L^*$ satisfy*

$$a_L^{(\ell)}\left(\frac{\partial^\ell u}{\partial x^\ell}\right)_L^* + b_L^{(\ell)}\left(\frac{\partial^\ell p}{\partial x^\ell}\right)_L^* = d_L^\ell, \tag{3.33}$$

and

$$g_{\rho L}^{(\ell)}\left(\frac{\partial^\ell \rho}{\partial x^\ell}\right)_L^* = g_{pL}^{(\ell)}\left(\frac{\partial^\ell p}{\partial x^\ell}\right)_L^* + h_L^{(\ell)}, \tag{3.34}$$

where the coefficients in (3.33) are

$$\begin{aligned}
&a_L^{(\ell)} = \left(2c_L^*\right)^\ell, \qquad b_L^{(\ell)} = \frac{2}{\rho_L^*}\left(2c_L^*\right)^{\ell-1},\\
&d_L^{(1)} = -\left(\frac{D_-\psi}{Dt}\right)_L^* + K_L^*\left(\frac{D_- S}{Dt}\right)_L^* - \left(\frac{A'}{A}cu\right)_L^*,\\
&d_L^{(2)} = \left[\frac{D_-^2\psi}{Dt^2} - K\frac{D_-^2 S}{Dt^2} - \frac{D_- K}{Dt}\frac{D_- S}{Dt}\right]_L^* + 2\left(\frac{\partial u}{\partial x}\right)_L^*\left[\frac{D_- c}{Dt} - c\frac{\partial u}{\partial x} - \frac{1}{\rho}\frac{\partial}{\partial x}\left(p+\rho c^2\right)\right]_L^*\\
&\qquad + 2\left(\frac{\partial p}{\partial x}\right)_L^*\left[\frac{\partial}{\partial t}\left(\frac{1}{\rho}\right) + (u-2c)\frac{\partial}{\partial x}\left(\frac{1}{\rho}\right)\right]_L^* - \left[\frac{\partial}{\partial x}\left(\frac{A'}{A}\rho c^2 u\right) - \frac{D_-}{Dt}\left(\frac{A'}{A}cu\right)\right]_L^*;
\end{aligned}$$

and the coefficients in (3.34) are

$$g_{\rho L}^{(\ell)} = (c_L^*)^\ell \left(\frac{\partial S}{\partial \rho}\right)_L^*, \qquad g_{pL}^{(\ell)} = -(c_L^*)^\ell \left(\frac{\partial S}{\partial p}\right)_L^*, \qquad h_L^{(1)} = -\left(\frac{D_- S}{Dt}\right)_L^*,$$
$$h_L^{(2)} = \left[\frac{D_-^2 S}{Dt^2} + \frac{D_- c}{Dt}\frac{\partial S}{\partial x} - c\frac{\partial u}{\partial x}\frac{\partial S}{\partial x}\right]_L^* - (c_L^*)^2\left[\frac{\partial}{\partial x}\left(\frac{\partial S}{\partial \rho}\right)\frac{\partial \rho}{\partial x} + \frac{\partial}{\partial x}\left(\frac{\partial S}{\partial p}\right)\frac{\partial p}{\partial x}\right]_L^*.$$

Proof. In the smooth region on the left side of contact wave Γ_0, we have from the definition of directional derivative $\frac{D_-}{Dt}$ and (2.2) that

$$\begin{cases} \dfrac{D_-\rho}{Dt} = -c\dfrac{\partial \rho}{\partial x} - \rho\dfrac{\partial u}{\partial x} - \dfrac{A'}{A}\rho u, \\ \dfrac{D_- u}{Dt} = -c\dfrac{\partial u}{\partial x} - \dfrac{1}{\rho}\dfrac{\partial p}{\partial x}, \\ \dfrac{D_- p}{Dt} = -c\dfrac{\partial p}{\partial x} - \rho c^2\dfrac{\partial u}{\partial x} - \dfrac{A'}{A}\rho c^2 u. \end{cases} \tag{3.35}$$

Inserting the $\frac{D_- u}{Dt}$ and $\frac{D_- p}{Dt}$ in (3.35) into the first equation of (2.7), we obtain

$$2c\frac{\partial u}{\partial x} + \frac{2}{\rho}\frac{\partial p}{\partial x} = -\frac{D_-\psi}{Dt} + K\frac{D_- S}{Dt} - \frac{A'}{A}cu. \tag{3.36}$$

This yields (3.33) for $\ell = 1$.

Furthermore, we act $\frac{D_-}{Dt}$ on the above equation to get

$$\begin{aligned} &2c\frac{D_-}{Dt}\left(\frac{\partial u}{\partial x}\right) + 2\frac{D_- c}{Dt}\frac{\partial u}{\partial x} + \frac{2}{\rho}\frac{D_-}{Dt}\left(\frac{\partial p}{\partial x}\right) + \frac{D_-}{Dt}\left(\frac{2}{\rho}\right)\frac{\partial p}{\partial x} \\ &\quad = -\frac{D_-^2\psi}{Dt^2} + K\frac{D_-^2 S}{Dt^2} + \frac{D_- K}{Dt}\frac{D_- S}{Dt} - \frac{D_-}{Dt}\left(\frac{A'}{A}cu\right), \end{aligned} \tag{3.37}$$

and apply $\frac{\partial}{\partial x}$ to the second and third equations of (3.35) to yield

$$\frac{D_-}{Dt}\left(\frac{\partial u}{\partial x}\right) = -c\frac{\partial^2 u}{\partial x^2} - \frac{1}{\rho}\frac{\partial^2 p}{\partial x^2} - \left(\frac{\partial u}{\partial x}\right)^2 - \frac{\partial}{\partial x}\left(\frac{1}{\rho}\right)\frac{\partial p}{\partial x}, \tag{3.38}$$

and

$$\frac{D_-}{Dt}\left(\frac{\partial p}{\partial x}\right) = -c\frac{\partial^2 p}{\partial x^2} - \rho c^2\frac{\partial^2 u}{\partial x^2} - \frac{\partial u}{\partial x}\frac{\partial}{\partial x}(p + \rho c^2) - \frac{\partial}{\partial x}\left(\frac{A'}{A}\rho c^2 u\right), \tag{3.39}$$

respectively. Inserting (3.38) and (3.39) into (3.37) enables us to obtain (3.33) for $\ell = 2$.

Finally, by making use of (2.4), we have

$$\frac{D_- S}{Dt} = -c\frac{\partial S}{\partial x} = -c\frac{\partial S}{\partial \rho}\frac{\partial \rho}{\partial x} - c\frac{\partial S}{\partial p}\frac{\partial p}{\partial x}, \tag{3.40}$$

and

$$\begin{aligned} \frac{D_-^2 S}{Dt^2} &= -\frac{D_- c}{Dt}\frac{\partial S}{\partial x} - c\frac{D_-}{Dt}\left(\frac{\partial S}{\partial x}\right) \\ &= -\frac{D_- c}{Dt}\frac{\partial S}{\partial x} + c\left(\frac{\partial u}{\partial x}\frac{\partial S}{\partial x} + c\frac{\partial^2 S}{\partial x^2}\right) \\ &= -\frac{D_- c}{Dt}\frac{\partial S}{\partial x} + c\frac{\partial u}{\partial x}\frac{\partial S}{\partial x} + c^2\left[\frac{\partial}{\partial x}\left(\frac{\partial S}{\partial \rho}\right)\frac{\partial \rho}{\partial x} + \frac{\partial}{\partial x}\left(\frac{\partial S}{\partial p}\right)\frac{\partial p}{\partial x}\right] + c^2\left(\frac{\partial S}{\partial \rho}\frac{\partial^2 \rho}{\partial x^2} + \frac{\partial S}{\partial p}\frac{\partial^2 p}{\partial x^2}\right). \end{aligned} \tag{3.41}$$

Then (3.34) follows from (3.40) and (3.41) for $\ell = 1$ and $\ell = 2$, respectively. □

Remark 3.3. If the λ_+-rarefaction wave, say Γ_+, is involved in the configuration, it can be resolved similarly by deriving the linear and quadratic GRP equations for $\boldsymbol{w}_+$. However, a better choice for us is to use the following property of system (2.1): (2.1) holds true under the transformation $\mathscr{T}: (\rho, u, p, A)(x,t) \to (\rho, -u, p, A)(-x,t)$. In fact, if we define $\tilde{Q} := \mathscr{T}(Q)$, then $\tilde{U}_L^* = \mathscr{T}(U_R^*)$, $\tilde{U}_L^* = \mathscr{T}(U_R^*)$, $\lambda_-(\tilde{U}_R^*) = \lambda_+(U_L^*)$ and Γ_+ corresponds to a left rarefaction wave of $\tilde{U}$, which can be resolved to obtain

$$\tilde{a}_L^{(\ell)}\left(\frac{\partial^\ell \tilde{u}}{\partial x^\ell}\right)_L^* + \tilde{b}_L^{(\ell)}\left(\frac{\partial^\ell \tilde{p}}{\partial x^\ell}\right)_L^* = \tilde{d}_L^\ell, \tag{3.42}$$

and

$$\tilde{g}_{\rho L}^{(\ell)}\left(\frac{\partial^\ell \tilde{\rho}}{\partial x^\ell}\right)_L^* = \tilde{g}_{pL}^{(\ell)}\left(\frac{\partial^\ell \tilde{p}}{\partial x^\ell}\right)_L^* + \tilde{h}_L^{(\ell)}, \tag{3.43}$$

for $\ell = 1, 2$. Note that

$$\left(\frac{\partial^\ell Q}{\partial x^\ell}\right)_R^* = (-1)^\ell\left(\left(\frac{\partial^\ell \tilde{\rho}}{\partial x^\ell}\right)_L^*, -\left(\frac{\partial^\ell \tilde{u}}{\partial x^\ell}\right)_L^*, \left(\frac{\partial^\ell \tilde{p}}{\partial x^\ell}\right)_L^*\right).$$

Then the linear equations analogous to (3.33) and (3.34) for $(\frac{\partial^\ell Q}{\partial x^\ell})_R^*$ are derived from (3.42) and (3.43).

4. Resolution of curved discontinuities

This section will give the resolution of the discontinuity waves, including the contact discontinuity and the shock wave. For each discontinuity wave, a set of linear equations for derivatives of the state variables will be obtained.

4.1. The shock wave

Let $x = x_s(t)$ be the shock trajectory associated with the third characteristic field and assume that it propagates with speed $s := x_s'(t)$. See Fig. 2.1(a). Denote the left and right states of the shock wave by U and $\bar{U}$, respectively, i.e., $U(t) := U(x_s(t-0), 0)$ and $\bar{U}(t) := U(x_s(t+0), 0)$. Across this shock, the Rankine–Hugoniot relation can be written in the form:

$$\begin{cases} \eta(p, u, \bar{p}, \bar{u}, \bar{\rho}) = 0, \\ \zeta(\rho, p, \bar{\rho}, \bar{p}) = 0, \end{cases} \tag{4.1}$$

and the shock speed s is given by

$$s = \frac{\rho u - \bar{\rho}\bar{u}}{\rho - \bar{\rho}}. \tag{4.2}$$

For the polytropic cases, η and ζ are given explicitly by

$$\eta = (p-\bar{p})^2 - \frac{\bar{\rho}}{2}(u-\bar{u})^2\big[(\gamma+1)p + (\gamma-1)\bar{p}\big],$$
$$\zeta = \big[(\gamma-1)p + (\gamma+1)\bar{p}\big]\rho - \big[(\gamma+1)p + (\gamma-1)\bar{p}\big]\bar{\rho}.$$

Differentiating (4.1) along the shock trajectory $x = x_s(t)$ gives

$$\begin{cases} \Pi_p^{(\ell)}\dfrac{D_s^\ell p}{Dt} + \Pi_u^{(\ell)}\dfrac{D_s^\ell u}{Dt} = \Pi_{rhs}^{(\ell)}, \\ \Lambda_\rho^{(\ell)}\dfrac{D_s^\ell \rho}{Dt} + \Lambda_p^{(\ell)}\dfrac{D_s^\ell p}{Dt} = \Lambda_{rhs}^{(\ell)}, \end{cases} \tag{4.3}$$

for $\ell = 1, 2$, where the operator $\frac{D_s}{Dt}$ is defined by $\frac{D_s}{Dt} := \frac{\partial}{\partial t} + s\frac{\partial}{\partial x}$ and the coefficients in the right hand side of (4.3) are given by

$$\begin{aligned} &\Pi_p^{(\ell)} = \frac{\partial \eta}{\partial p}, \qquad \Pi_u^{(\ell)} = \frac{\partial \eta}{\partial u}, \qquad \Pi_{rhs}^{(1)} = -\frac{\partial \eta}{\partial \bar{p}}\frac{D_s\bar{p}}{Dt} - \frac{\partial \eta}{\partial \bar{u}}\frac{D_s\bar{u}}{Dt} - \frac{\partial \eta}{\partial \bar{\rho}}\frac{D_s\bar{\rho}}{Dt}, \\ &\Pi_{rhs}^{(2)} = -\frac{D_s}{Dt}\left(\frac{\partial \eta}{\partial p}\right)\frac{D_s p}{Dt} - \frac{D_s}{Dt}\left(\frac{\partial \eta}{\partial u}\right)\frac{D_s u}{Dt} - \frac{D_s}{Dt}\left(\frac{\partial \eta}{\partial \bar{p}}\right)\frac{D_s\bar{p}}{Dt} \\ &\qquad - \frac{\partial \eta}{\partial \bar{p}}\frac{D_s^2\bar{p}}{Dt^2} - \frac{D_s}{Dt}\left(\frac{\partial \eta}{\partial \bar{u}}\right)\frac{D_s\bar{u}}{Dt} - \frac{\partial \eta}{\partial \bar{u}}\frac{D_s^2\bar{u}}{Dt^2} - \frac{D_s}{Dt}\left(\frac{\partial \eta}{\partial \bar{\rho}}\right)\frac{D_s\bar{\rho}}{Dt} - \frac{\partial \eta}{\partial \bar{\rho}}\frac{D_s^2\bar{\rho}}{Dt^2}; \end{aligned} \tag{4.4}$$

and

$$\begin{aligned} &\Lambda_\rho^{(\ell)} = \frac{\partial \zeta}{\partial \rho}, \qquad \Lambda_p^{(\ell)} = \frac{\partial \zeta}{\partial p}, \qquad \Lambda_{rhs}^{(1)} = -\frac{\partial \zeta}{\partial \bar{\rho}}\frac{D_s\bar{\rho}}{Dt} - \frac{\partial \zeta}{\partial \bar{p}}\frac{D_s\bar{p}}{Dt}, \\ &\Lambda_{rhs}^{(2)} = -\frac{D_s}{Dt}\left(\frac{\partial \zeta}{\partial \rho}\right)\frac{D_s\rho}{Dt} - \frac{D_s}{Dt}\left(\frac{\partial \zeta}{\partial p}\right)\frac{D_s p}{Dt} - \frac{D_s}{Dt}\left(\frac{\partial \zeta}{\partial \bar{\rho}}\right)\frac{D_s\bar{\rho}}{Dt} - \frac{\partial \zeta}{\partial \bar{\rho}}\frac{D_s^2\bar{\rho}}{Dt^2} - \frac{D_s}{Dt}\left(\frac{\partial \zeta}{\partial \bar{p}}\right)\frac{D_s\bar{p}}{Dt} - \frac{\partial \zeta}{\partial \bar{p}}\frac{D_s^2\bar{p}}{Dt^2}. \end{aligned} \tag{4.5}$$

Remark 4.1. For the polytropic cases, the coefficients in (4.4) are

$$\begin{aligned}
&\Pi_p^{(\ell)} = 2(p-\bar p) - \frac{\gamma+1}{2}\bar\rho p(u-\bar u), \qquad \Pi_u^{(\ell)} = -\bar\rho(u-\bar u)\big[(\gamma+1)p+(\gamma-1)\bar p\big],\\
&\Pi_{rhs}^{(1)} = \left[2(p-\bar p)+\frac{\gamma-1}{2}\bar\rho(u-\bar u)^2\right]\frac{D_s\bar p}{Dt}\\
&\qquad + \left[\frac{1}{2}(u-\bar u)\frac{D_s\rho}{Dt} - \bar\rho\frac{D_s\bar u}{Dt}\right](u-\bar u)\big[(\gamma+1)p+(\gamma-1)\bar p\big],\\
&\Pi_{rhs}^{(2)} = \big[(\gamma+1)p+(\gamma-1)\bar p\big]\left[\frac{(u-\bar u)^2}{2}\frac{D_s^2\bar\rho}{Dt^2} - \bar\rho(u-\bar u)\frac{D_s^2\bar u}{Dt^2}\right]\\
&\qquad + \left[2(p-\bar p)+\frac{\gamma-1}{2}\bar\rho(u-\bar u)^2\right]\frac{D_s^2\bar p}{Dt^2} - 2\left[\frac{D_-}{Dt}(p-\bar p)\right]^2\\
&\qquad - \big[(\gamma+1)p+(\gamma-1)\bar p\big]\frac{D_s}{Dt}(u-\bar u)\left[2(u-\bar u)\frac{D_s\bar\rho}{Dt}+\bar\rho\frac{D_s}{Dt}(u-\bar u)\right]\\
&\qquad + (u-\bar u)\left[(\gamma+1)\frac{D_sp}{Dt}+(\gamma-1)\frac{D_s\bar p}{Dt}\right]\left[2\bar\rho\frac{D_s}{Dt}(u-\bar u)+\frac{D_s\bar\rho}{Dt}(u-\bar u)\right];
\end{aligned}$$

and the coefficients in (4.5) are

$$\begin{aligned}
&\Lambda_\rho^{(\ell)} = (\gamma-1)p+(\gamma+1)\bar p, \qquad \Lambda_p^{(\ell)} = (\gamma-1)\rho-(\gamma+1)\bar\rho,\\
&\Lambda_{rhs}^{(1)} = \big[-(\gamma+1)\rho+(\gamma-1)\bar\rho\big]\frac{D_s\bar p}{Dt} + \big[(\gamma+1)p+(\gamma-1)\bar p\big]\frac{D_s\bar\rho}{Dt},\\
&\Lambda_{rhs}^{(2)} = \big[(\gamma+1)p+(\gamma-1)\bar p\big]\frac{D_s^2\bar\rho}{Dt^2} + \left[(\gamma+1)\frac{D_sp}{Dt}+(\gamma-1)\frac{D_s\bar p}{Dt}\right]\frac{D_s\bar\rho}{Dt}\\
&\qquad + \big[(\gamma-1)\bar\rho-(\gamma+1)\rho\big]\frac{D_s^2\bar p}{Dt^2} - \left[(\gamma-1)\frac{D_s\rho}{Dt}+(\gamma+1)\frac{D_s\bar\rho}{Dt}\right]\frac{D_sp}{Dt}.
\end{aligned}$$

Next, we express the $\frac{D_s^\ell\rho}{Dt^\ell}$, $\frac{D_s^\ell u}{Dt^\ell}$ and $\frac{D_s^\ell p}{Dt^\ell}$ $(\ell=1,2)$ in (4.3) in terms of the corresponding spatial derivatives as

$$\begin{aligned}
&\frac{D_s\rho}{Dt} = -(u-s)\frac{\partial\rho}{\partial x} - \rho\frac{\partial u}{\partial x} + C_\rho^{(1)},\\
&\frac{D_su}{Dt} = -(u-s)\frac{\partial u}{\partial x} - \frac{1}{\rho}\frac{\partial p}{\partial x},\\
&\frac{D_sp}{Dt} = -(u-s)\frac{\partial p}{\partial x} - \rho c^2\frac{\partial u}{\partial x} + C_p^{(1)};
\end{aligned} \tag{4.6}$$

and

$$\begin{aligned}
&\frac{D_s^2\rho}{Dt^2} = (u-s)^2\frac{\partial^2\rho}{\partial x^2} + 2\rho(u-s)\frac{\partial^2u}{\partial x^2} + \frac{\partial^2p}{\partial x^2} + C_\rho^{(2)},\\
&\frac{D_s^2u}{Dt^2} = \big[(u-s)^2+c^2\big]\frac{\partial^2u}{\partial x^2} + \frac{2(u-s)}{\rho}\frac{\partial^2p}{\partial x^2} + C_u^{(2)},\\
&\frac{D_s^2p}{Dt^2} = \big[(u-s)^2+c^2\big]\frac{\partial^2p}{\partial x^2} + 2(u-s)\rho c^2\frac{\partial^2u}{\partial x^2} + C_p^{(2)},
\end{aligned} \tag{4.7}$$

where

$$\begin{aligned}
&C_\rho^{(1)} = -\frac{A'}{A}\rho u, \qquad C_p^{(1)} = -\frac{A'}{A}\rho c^2u,\\
&C_\rho^{(2)} = \left[\frac{D_ss}{Dt}+4(u-s)\frac{\partial u}{\partial x}\right]\frac{\partial\rho}{\partial x} + 2\rho\left(\frac{\partial u}{\partial x}\right)^2 + \frac{\partial}{\partial t}\left(\frac{A'}{A}\rho u\right) + \left(u+\frac{\partial u}{\partial x}\right)\frac{\partial}{\partial x}\left(\frac{A'}{A}\rho u\right),\\
&C_u^{(2)} = \frac{\partial u}{\partial x}\left[\frac{D_ss}{Dt}+2(u-s)\frac{\partial u}{\partial x}+\frac{1}{\rho}\frac{\partial}{\partial x}\big(p+\rho c^2\big)\right]\\
&\qquad + \frac{\partial p}{\partial x}\left[\frac{\partial}{\partial t}\left(\frac{1}{\rho}\right)+(u-2s)\frac{\partial}{\partial x}\left(\frac{1}{\rho}\right)\right] + \frac{1}{\rho}\frac{\partial}{\partial x}\left(\frac{A'}{A}\rho c^2u\right),
\end{aligned}$$

$$C_p^{(2)} = \frac{\partial p}{\partial x}\left[\frac{D_s s}{Dt} + 2(u-s)\frac{\partial u}{\partial x} + \frac{1}{\rho}\left(\frac{\partial p}{\partial x} - c^2\frac{\partial \rho}{\partial x}\right)\right] - \frac{\partial u}{\partial x}\left[\frac{\partial(\rho c^2)}{\partial t} - (u-2s)\frac{\partial(\rho c^2)}{\partial x} - \rho c^2\frac{\partial \rho}{\partial x}\right] - \frac{\partial}{\partial t}\left(\frac{A'}{A}\rho c^2 u\right) + (u-2s)\frac{\partial}{\partial x}\left(\frac{A'}{A}\rho c^2 u\right).$$

By inserting (4.6) and (4.7) into (4.3) and then taking the limit $t \to 0^+$, we can get the following lemma.

Lemma 4.1. *For $\ell = 1, 2$, the limiting values $(\frac{\partial^\ell u}{\partial x^\ell})^*_R$, $(\frac{\partial^\ell p}{\partial x^\ell})^*_R$ and $(\frac{\partial^\ell \rho}{\partial x^\ell})^*_R$ satisfy*

$$a_R^{(\ell)}\left(\frac{\partial^\ell u}{\partial x^\ell}\right)^*_R + b_R^{(\ell)}\left(\frac{\partial^\ell p}{\partial x^\ell}\right)^*_R = d_R^{(\ell)}, \tag{4.8}$$

and

$$g_{\rho R}^{(\ell)}\left(\frac{\partial^\ell \rho}{\partial x^\ell}\right)^*_R = g_{pR}^{(\ell)}\left(\frac{\partial^\ell p}{\partial x^\ell}\right)^*_R + g_{uR}^{(\ell)}\left(\frac{\partial^\ell u}{\partial x^\ell}\right)^*_R + h_R^{(\ell)}, \tag{4.9}$$

where the coefficients in (4.8) are, for $\ell = 1$,

$$a_R^{(1)} = -(u-s)\Pi_u^{(1)} - \rho c^2\Pi_p^{(1)}, \qquad b_R^{(1)} = -(u-s)\Pi_p^{(1)} - \frac{1}{\rho}\Pi_u^{(1)}, \qquad d_R^{(1)} = \Pi_{rhs}^{(1)} - c_p^{(1)}\Pi_p^{(1)};$$

and for $\ell = 2$,

$$a_R^{(2)} = -\left[(u-s)^2 + c^2\right]\Pi_u^{(2)} + 2(u-s)\rho c^2\Pi_p^{(2)},$$
$$b_R^{(2)} = -\frac{2(u-s)}{\rho}\Pi_u^{(2)} + \left[(u-s)^2 + c^2\right]\Pi_p^{(2)},$$
$$d_R^{(2)} = \Pi_{rhs}^{(2)} - C_u^{(2)}\Pi_u^{(2)} - C_p^{(2)}\Pi_p^{(2)}.$$

The coefficients in (4.9) are, for $\ell = 1$,

$$g_{\rho R}^{(1)} = -(u-s)\Lambda_\rho^{(1)}, \qquad g_{uR}^{(1)} = \rho\Lambda_\rho^{(1)} + \rho c^2\Lambda_p^{(1)},$$
$$g_{pR}^{(1)} = (u-s)\Lambda_p^{(1)}, \qquad h_R^{(1)} = \Lambda_{rhs}^{(1)} - C_\rho^{(1)}\Lambda_\rho^{(1)} - C_p^{(1)}\Lambda_p^{(1)};$$

and for $\ell = 2$,

$$g_{\rho R}^{(2)} = (u-s)^2\Lambda_\rho^{(2)}, \qquad g_{uR}^{(2)} = 2\rho(u-s)\left(\rho c^2\Lambda_p^{(2)} - \Lambda_\rho^{(2)}\right),$$
$$g_{pR}^{(2)} = \left[(u-s)^2 + c^2\right]\Lambda_p^{(2)} + \Lambda_\rho^{(2)}, \qquad h_R^{(2)} = \Lambda_{rhs}^{(2)} - C_\rho^{(2)}\Lambda_\rho^{(2)} - C_p^2\Lambda_p^{(2)}.$$

In the above coefficients, the variables U, $\bar{U}$, $\frac{\partial U}{\partial x}$ and $\frac{\partial^\ell \bar{U}}{\partial x^\ell}$ $(\ell = 1, 2)$ involved all take values at $t = 0^+$, i.e.,

$$U = U_R^*, \qquad \bar{U} = U_R, \qquad \frac{\partial U}{\partial x} = \left(\frac{\partial U}{\partial x}\right)^*_R, \qquad \frac{\partial^\ell \bar{U}}{\partial x^\ell} = \left(\frac{\partial^\ell U}{\partial x^\ell}\right)_R.$$

4.2. The contact discontinuity

Now let us denote by $x = x_c(t)$ the trajectory of the contact discontinuity wave Γ_0 with the propagation speed $x_c'(t) = u$. Across this contact discontinuity, the GRI, p and u, remain continuous. Thus differentiating u and p along $x = x_c(t)$ gives, respectively,

$$\left(\frac{D^\ell u}{Dt^\ell}\right)^*_L = \left(\frac{D^\ell u}{Dt^\ell}\right)^*_R \quad \text{and} \quad \left(\frac{D^\ell p}{Dt^\ell}\right)^*_L = \left(\frac{D^\ell p}{Dt^\ell}\right)^*_R. \tag{4.10}$$

Similar to the resolution of the shock wave in Section 4.1, we express $\frac{D^\ell u}{Dt^\ell}$ and $\frac{D^\ell p}{Dt^\ell}$ $(\ell = 1, 2)$ as

$$\frac{Du}{Dt} = -\frac{1}{\rho}\frac{\partial p}{\partial x}, \qquad \frac{Dp}{Dt} = -\rho c^2\frac{\partial u}{\partial x} - \frac{A'}{A}\rho c^2 u, \tag{4.11}$$

and

$$\frac{D^2 u}{Dt^2} = c^2\frac{\partial^2 u}{\partial x^2} + I_u, \qquad \frac{D^2 p}{Dt^2} = c^2\frac{\partial^2 p}{\partial x^2} + I_p, \tag{4.12}$$

where

$$I_u = -\frac{D\rho}{Dt}\frac{\partial p}{\partial x} + \frac{1}{\rho}\frac{\partial u}{\partial x}\frac{\partial}{\partial x}\left(u + \rho c^2\right),$$
$$I_p = -\frac{D(\rho c^2)}{Dt}\frac{\partial u}{\partial x} + \rho c^2\left(\frac{\partial u}{\partial x}\right)^2 - \frac{c^2}{\rho}\frac{\partial \rho}{\partial x}\frac{\partial p}{\partial x} - \frac{D}{Dt}\left(\frac{A'}{A}\rho c^2 u\right).$$

Then we arrive at the following lemma.

Lemma 4.2. *For $\ell = 1, 2$, the limiting values $(\frac{\partial^\ell u}{\partial x^\ell})^*_{L/R}$ and $(\frac{\partial^\ell p}{\partial x^\ell})^*_{L/R}$ satisfy*

$$\left(e_u^{(\ell)}\right)^*_L\left(\frac{\partial^\ell u}{\partial x^\ell}\right)^*_L - \left(e_u^{(\ell)}\right)^*_R\left(\frac{\partial^\ell u}{\partial x^\ell}\right)^*_R = f_u^{(\ell)},$$
$$\left(e_p^{(\ell)}\right)^*_L\left(\frac{\partial^\ell p}{\partial x^\ell}\right)^*_L - \left(e_p^{(\ell)}\right)^*_R\left(\frac{\partial^\ell p}{\partial x^\ell}\right)^*_R = f_p^{(\ell)}, \tag{4.13}$$

where

$$e_u^{(\ell)} = c^2\rho^{2-\ell}, \qquad e_p^{(\ell)} = c^2\left(\rho c^2\right)^{\ell-2},$$

and

$$f_u^{(1)} = \frac{A'}{A}\left[\left(\rho c^2 u\right)^*_R - \left(\rho c^2 u\right)^*_L\right], \qquad f_u^{(2)} = (I_u)^*_R - (I_u)^*_L, \qquad f_p^{(2)} = (I_p)^*_R - (I_p)^*_L.$$

5. The GRP solvers

In this section, we will present the full solvers for the linear and quadratic GRP using the results in Sections 3 and 4.

5.1. The nonsonic case

As the t-axis is not located in the rarefaction wave, we have the nonsonic case. In each subregion apart from the rarefaction wave, the flow is smooth and the time derivatives $\frac{\partial Q}{\partial t}$ and $\frac{\partial^2 Q}{\partial t^2}$ can be derived from the spatial derivative $\frac{\partial Q}{\partial x}$ and $\frac{\partial^2 Q}{\partial x^2}$. Indeed, Eq. (2.2) gives

$$\frac{\partial Q}{\partial t} = -J\frac{\partial Q}{\partial x} + H := \mathcal{A}^{(1)}\left(Q, \frac{\partial Q}{\partial x}\right). \tag{5.1}$$

Furthermore, by applying $\frac{\partial}{\partial x}$ and $\frac{\partial}{\partial t}$ to (2.2), we get

$$\frac{\partial^2 Q}{\partial t\partial x} = J\frac{\partial^2 Q}{\partial x^2} - \frac{\partial J}{\partial x}\frac{\partial Q}{\partial x} + \frac{\partial H}{\partial t}, \tag{5.2}$$
$$\frac{\partial^2 Q}{\partial t^2} = -J\frac{\partial^2 Q}{\partial t\partial x} - \frac{\partial J}{\partial t}\frac{\partial Q}{\partial x} + \frac{\partial H}{\partial t}. \tag{5.3}$$

Insert (5.1) and (5.2) into (5.3). Then $\frac{\partial^2 Q}{\partial t^2}$ can be expressed as a function of Q, $\frac{\partial Q}{\partial x}$ and $\frac{\partial^2 Q}{\partial x^2}$:

$$\frac{\partial^2 Q}{\partial t^2} = \mathcal{A}^{(2)}\left(Q, \frac{\partial Q}{\partial x}, \frac{\partial^2 Q}{\partial x^2}\right). \tag{5.4}$$

Therefor for the nonsonic case, it suffices for us to solve the spatial derivatives $\frac{\partial^\ell Q}{\partial x^\ell}$ $(\ell = 1, 2)$, and treat the case that the t-axis lies in the intermediate region of Γ_- and Γ_+, since the $\frac{\partial^\ell Q}{\partial x^\ell}$ are determined by the initial data (2.10) on the left (resp. right) of Γ_- (resp. Γ_+).

For the nonsonic case, we summarize the resolution of the linear and quadratic GRP in the following proposition.

Proposition 5.1 *(Linear and quadratic GRP: Nonsonic case). Assume that the configuration is as shown in Fig. 2.1*(a) *and the t-axis is located in either of the two intermediate subregions. Then the limiting values $(\frac{\partial^\ell u}{\partial x^\ell})^*_{L/R}$ and $(\frac{\partial^\ell p}{\partial x^\ell})^*_{L/R}$, for $\ell = 1, 2$, can be obtained by solving a set linear algebraic equations*:

$$\begin{cases} a_L^{(\ell)}\left(\dfrac{\partial^\ell u}{\partial x^\ell}\right)_L^* + b_L^{(\ell)}\left(\dfrac{\partial^\ell p}{\partial x^\ell}\right)_L^* = d_L^\ell, \\ a_R^{(\ell)}\left(\dfrac{\partial^\ell u}{\partial x^\ell}\right)_R^* + b_R^{(\ell)}\left(\dfrac{\partial^\ell p}{\partial x^\ell}\right)_R^* = d_R^{(\ell)}, \\ \left(e_u^{(\ell)}\right)_L^*\left(\dfrac{\partial^\ell u}{\partial x^\ell}\right)_L^* - \left(e_u^{(\ell)}\right)_R^*\left(\dfrac{\partial^\ell u}{\partial x^\ell}\right)_R^* = f_u^{(\ell)}, \\ \left(e_p^{(\ell)}\right)_L^*\left(\dfrac{\partial^\ell p}{\partial x^\ell}\right)_L^* - \left(e_p^{(\ell)}\right)_R^*\left(\dfrac{\partial^\ell p}{\partial x^\ell}\right)_R^* = f_p^{(\ell)}; \end{cases} \tag{5.5}$$

and $(\frac{\partial^\ell \rho}{\partial x^\ell})_L^*$ *and* $(\frac{\partial^\ell \rho}{\partial x^\ell})_R^*$ *can be determined by*

$$g_{\rho L}^{(\ell)}\left(\frac{\partial^\ell \rho}{\partial x^\ell}\right)_L^* = g_{pL}^{(\ell)}\left(\frac{\partial^\ell p}{\partial x^\ell}\right)_L^* + h_L^{(\ell)}, \tag{5.6}$$

and

$$g_{\rho R}^{(\ell)}\left(\frac{\partial^\ell \rho}{\partial x^\ell}\right)_R^* = g_{pR}^{(\ell)}\left(\frac{\partial^\ell p}{\partial x^\ell}\right)_R^* + g_{uR}^{(\ell)}\left(\frac{\partial^\ell u}{\partial x^\ell}\right)_R^* + h_R^{(\ell)}, \tag{5.7}$$

respectively, where the coefficients in (5.5), (5.6) *and* (5.7) *are defined in Lemmas* 3.4, 4.2 *and* 4.1.

If $u_* > 0$, $(\frac{\partial^\ell Q}{\partial x^\ell})_* = (\frac{\partial^\ell Q}{\partial x^\ell})_L^*$. *Otherwise, if* $u_* < 0$, $(\frac{\partial^\ell Q}{\partial x^\ell})_* = (\frac{\partial^\ell Q}{\partial x^\ell})_R^*$. *Having solved* $(\frac{\partial Q}{\partial x})_*$ *and* $(\frac{\partial^2 Q}{\partial x^2})_*$, *the time derivatives* $(\frac{\partial Q}{\partial t})_*$ *and* $(\frac{\partial^2 Q}{\partial t^2})_*$ *are given by*

$$\left(\frac{\partial Q}{\partial t}\right)_* = \mathcal{A}^{(1)}\left(Q_*, \left(\frac{\partial Q}{\partial x}\right)_*\right),$$

and

$$\left(\frac{\partial^2 Q}{\partial t^2}\right)_* = \mathcal{A}^{(2)}\left(Q_*, \left(\frac{\partial Q}{\partial x}\right)_*, \left(\frac{\partial^2 Q}{\partial x^2}\right)_*\right),$$

respectively.

5.2. The sonic case

As far as the sonic case is concerned, the t-axis is located in the left rarefaction fan and is in fact tangential to the λ_--characteristic curve with zero initial slope, i.e., $\lambda_-(0) = 0$. By recalling the notation $\frac{D_- U}{Dt}(0, \beta)$ in Section 3, we have for $\beta_* = 0$,

$$\left(\frac{\partial U}{\partial t}\right)_* = \frac{D_- U}{Dt}(0, \beta_*). \tag{5.8}$$

Proposition 5.2 *(Linear GRP: Sonic case). Assuming that the t-axis is located inside the left rarefaction fan, we have for* $\beta_* = 0$,

$$\begin{aligned} \left(\frac{\partial u}{\partial t}\right)_* &= \frac{1}{2}\left(\frac{D_-\psi}{Dt}(0,\beta_*) - K_*\frac{D_- S}{Dt}(0,\beta_*) + \frac{A'}{A}u_* c_*\right), \\ \left(\frac{\partial p}{\partial t}\right)_* &= \frac{\rho_* c_*}{2}\left(\frac{D_-\psi}{Dt}(0,\beta_*) - K_*\frac{D_- S}{Dt}(0,\beta_*) - \frac{A'}{A}u_* c_*\right), \\ \left(\frac{\partial \rho}{\partial t}\right)_* &= \frac{1}{c_*}\left(\frac{\partial p}{\partial t}\right)_* + \left(\frac{\partial p}{\partial \rho}\right)_*\frac{\partial S}{\partial t}(0,\beta_*). \end{aligned} \tag{5.9}$$

Proof. For $(\frac{\partial u}{\partial t})_*$ and $(\frac{\partial p}{\partial t})_*$, from (2.6) we have

$$\left(\frac{D_- u}{Dt} + \frac{1}{\rho c}\frac{D_- p}{Dt}\right)(0,\beta_*) = \left(\frac{D_-\psi}{Dt} - K(\rho, S)\frac{D_- S}{Dt}\right)(0,\beta_*). \tag{5.10}$$

On the other hand, the third equation of (2.3) gives

$$\left(\frac{D_- u}{Dt} - \frac{1}{\rho c}\frac{D_- p}{Dt}\right)(0,\beta_*) = \frac{A'}{A}u_* c_*. \tag{5.11}$$

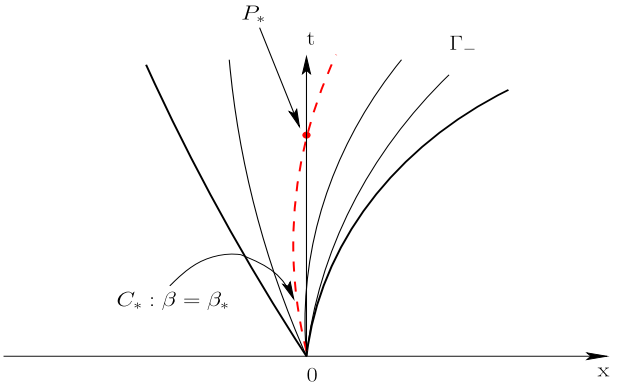

Fig. 5.1. The characteristic curve $\beta = \beta_*$, dashed line.

Then combining (5.10) and (5.11) gives the $(\frac{\partial u}{\partial t})_*$ and $(\frac{\partial p}{\partial t})_*$ in (5.9). The time derivative $(\frac{\partial \rho}{\partial t})_*$ can be obtained from

$$\left(\frac{D_- p}{Dt}\right)(0,\beta_*) = \left(c^2\frac{D_-\rho}{Dt} + \frac{\partial p}{\partial S}\frac{D_- S}{Dt}\right)(0,\beta_*). \qquad \square$$

We now proceed to resolve the quadratic GRP. Using the chain rule, we have

$$\frac{D_-^2 U}{Dt^2} = \frac{\partial^2 U}{\partial t^2} + \left(\frac{D_-\lambda_-}{Dt} + 2\lambda_-\frac{\partial U}{\partial t}\right)\frac{\partial U}{\partial x} + \lambda_-^2\left(\frac{\partial U}{\partial x}\right)^2. \tag{5.12}$$

As stated in Remark 3.1(ii), $\frac{D_-^2 U}{Dt^2}(0,\beta)$ takes a finite value in the rarefaction fan. However, the value of $\frac{\partial^2 U}{\partial t^2}$ (expect for $U = w_-$) in the right hand side of (5.12) tends to infinity as $t \to 0$ inside the rarefaction fan, as $\frac{\partial U}{\partial x}$ does. In order to get the third order approximation of U, it is impossible to apply the Taylor expansion (2.13) directly and we have to use a new method as follows. For any point $P_* = (0, \Delta t)$ with Δt being small, in order to evaluate $U(P_*)$, we need to find out the initial slope β_* of the characteristic curve C_* which emanates from the singularity and goes though P_*. See Fig. 5.1.

Proposition 5.3 *(Quadratic GRP: Sonic case). Assume that the t-axis is located inside the rarefaction wave associated with λ_- and denote by $\Phi = (S, \psi_-, \psi_+)$. Then for any point $P_* = (0, \Delta t)$ with Δt being small, we have*

$$\Phi(P_*) = \Phi(\beta_*) + \frac{D_-\Phi}{Dt}(\beta_*)\Delta t + \frac{D_-^2\Phi}{Dt^2}(\beta_*)\frac{\Delta t^2}{2} + O\left(\Delta t^3\right), \tag{5.13}$$

where β_* is the root of

$$\beta + \frac{D_-\lambda_-}{Dt}(\beta)\frac{\Delta t}{2} = 0. \tag{5.14}$$

Proof. Let C_* be the λ_--characteristic curve with initial slope β_*. Note that, for any $(x(t), t) \in C_*$, we have

$$x(t) = \int_0^t \lambda\, ds = \int_0^t \left(\lambda_-(0) + \frac{D_-\lambda_-}{Dt}(0)s + O\left(s^2\right)\right) ds. \tag{5.15}$$

As $\lambda_-(0) = \beta_*$ satisfies (5.14), from (5.15) we see that

$$x(\Delta t) = x(P_*) + O\left(\Delta t^3\right),$$

where $x(P_*) = 0$. It follows that

$$\Phi(P_*) = \Phi\left(x(\Delta t), \Delta t\right) + O\left(\Delta t^3\right).$$

Expanding $\Phi(x(\Delta t), \Delta t)$ in the above equation as the Taylor series with respect to Δt, we finally obtain (5.13). $\square$

Remark 5.1. For the polytropic cases, the formulae for $\frac{D_-^\ell \Phi}{Dt^\ell}$, $\ell = 1, 2$, are given in Lemma 3.3 and Remark 3.2. Besides, in order to solve (5.14), we use the Newton iteration with initial guess $\beta_* = 0$.

6. The acoustic approximation

As $U_- = U_+$ and $\frac{\partial^\ell P_-}{\partial x^\ell}(0^-) \neq \frac{\partial^\ell P_+}{\partial x^\ell}(0^+)$, we refer it to as the acoustic case. In this case, each of the three waves degenerates to a characteristic curve whose two side states are the same. In particular, as the initial data has a small jump $\|U_- - U_+\| \ll 1$, we adopt the *acoustic approximation* in the sense that U_- and U_+ are regarded as the same approximately.

For convenience, in this section we denote by $\lambda_k := u + (k-2)c$, $k = 1, 2, 3$, the three eigenvalues of the system (2.1) and by L_k, $k = 1, 2, 3$, the three left eigenvectors of $\hat{J} := \frac{\partial F^{total}}{\partial U}$. Moreover, the acoustic wave associated with λ_k is denoted by Γ_k and the operator $\frac{D_k}{Dt}$ is defined as $\frac{D_k}{Dt} := \frac{\partial}{\partial t} + \lambda_k \frac{\partial}{\partial x}$. For fixed k, the two side state of Γ_k are simply denoted by U_L and U_R.

For the acoustic wave Γ_k, we use the continuity property of U and make differentiation along Γ_k to obtain $(\frac{D_k U}{Dt})_L = (\frac{D_k U}{Dt})_R$. Then we proceed to use (2.1) to get

$$(\lambda_k I - \hat{J})_L \left(\frac{\partial U}{\partial x}\right)_L - \frac{A'}{A} F_L = (\lambda_k I - \hat{J})_R \left(\frac{\partial U}{\partial x}\right)_R - \frac{A'}{A} F_R. \tag{6.1}$$

Note that $U_L = U_R$. Then we find that (6.1) is equivalent to

$$L_j \left(\frac{\partial U}{\partial x}\right)_L = L_j \left(\frac{\partial U}{\partial x}\right)_R, \quad j \neq k. \tag{6.2}$$

Moreover, applying $\frac{D_k}{Dt}$ to (6.2) yields

$$(\lambda_k - \lambda_j) L_j \left[\left(\frac{\partial^2 U}{\partial x^2}\right)_R - \left(\frac{\partial^2 U}{\partial x^2}\right)_L\right] = \frac{D_k L_j}{Dt}\left[\left(\frac{\partial U}{\partial x}\right)_L - \left(\frac{\partial U}{\partial x}\right)_R\right] - L_j \left[\left(\frac{\partial \hat{J}}{\partial x}\frac{\partial U}{\partial x}\right)_L - \left(\frac{\partial \hat{J}}{\partial x}\frac{\partial U}{\partial x}\right)_R\right]. \tag{6.3}$$

In addition, if $(\frac{\partial U}{\partial x})_L = (\frac{\partial U}{\partial x})_R$, then (6.3) can be reduced to

$$L_j \left(\frac{\partial^2 U}{\partial x^2}\right)_L = L_j \left(\frac{\partial^2 U}{\partial x^2}\right)_R. \tag{6.4}$$

Interestingly, in the course of acoustic approximation, we can obtain $\frac{\partial^\ell U}{\partial x^\ell}$ equivalently by solving linear classical Riemann-type problems

$$\begin{cases} \dfrac{\partial}{\partial t}\left(\dfrac{\partial^\ell U}{\partial x^\ell}\right) + \hat{J}(U_*)\dfrac{\partial}{\partial x}\left(\dfrac{\partial^\ell U}{\partial x^\ell}\right) = 0, \\ \dfrac{\partial^\ell U}{\partial x^\ell}(x,0) = \begin{cases} \dfrac{\partial^\ell P_-}{\partial x^\ell}(0), & \text{if } x < 0, \\ \dfrac{\partial^\ell P_+}{\partial x^\ell}(0), & \text{if } x > 0, \end{cases} \end{cases} \tag{6.5}$$

with $U_* = (U_- + U_+)/2$. Note that $L_j \frac{\partial U}{\partial x}$ $(j \neq k)$ in (6.2), are nothing but the generalized Riemann invariants of system (6.5) associated with λ_k. In addition, if $\frac{\partial P_-}{\partial x}(0) \approx \frac{\partial P_+}{\partial x}(0)$, from (6.4), we see that $\frac{\partial^2 U}{\partial x^2}$ can also be approximated by solving (6.5) with $\ell = 2$. In general, we have the following proposition.

Proposition 6.1. *For any $m \geqslant 1$, assume that $\frac{\partial^\ell P_-}{\partial x^\ell}(0) = \frac{\partial^\ell P_+}{\partial x^\ell}(0)$ $(1 \leqslant \ell \leqslant m-1)$ and $P_-(0) = P_+(0)$. Then $\frac{\partial^m U}{\partial x^m}$ are determined by the linear system (6.5) with $\ell = m$.*

Remark 6.1. (i) As indicated by (6.5), the spatial derivative $\frac{\partial^m U}{\partial x^m}$ in Proposition 6.1 is independent of the source term. Besides, since U is smooth in the subregions separated by Γ_k, $k = 1, 2, 3$, the corresponding time derivatives $\frac{\partial^\ell U}{\partial t^\ell}$, $0 \leqslant \ell \leqslant m$, follow from the Cauchy–Kowalewski procedure as illustrated in [22].

(ii) Also we note that, under the acoustic assumption in Proposition 6.1, all the approximate DRP solvers proposed in [12,23,8] are valid and are actually equivalent to the present acoustic GRP solvers.

As for the resolution of GRP (2.1)–(2.10), if the initial data (2.10) has a jump discontinuity, we can derive the solvers analytically as in Section 5 to calculate the time derivatives of U, with possible acoustic approximation for a partial set of waves. This leads to the solver which we label as the LGRP$_\infty$ (QGRP$_\infty$) *solver*. While the jump $U_+ - U_-$ of U is very small, we can use (6.5) (or possibly (6.3)) to calculate the space derivatives approximately. The resulting solver is labeled as the LGRP$_1$ (QGRP$_1$) *solver*.

7. Tests for the GRP solvers

In this section we assess the performance of the GRP solvers for the compressible Euler equations system, i.e., (1.1) with $A(x) = 1$. The aim is to show, via several test problems, the accuracy and behavior of the present solvers. As tests, we use the generalized Riemann problems proposed by [8] and construct new test examples with large jumps in pressure. The first test has no jump discontinuities in the state variables but admits discontinuities in derivatives at the interface. The more demanding test problems are constructed from the first one, by adding a discontinuity in pressure. Six new cases are thus generated by varying the strength of the initial pressure jump $\Delta p = (p_L - p_R)/p_R$ at the interface, namely $\Delta p = 10^k$, $k = -2, \ldots, 3$. The last test problem for the sonic case are constructed by adding $\Delta u = 28$ to the initial flow velocity of the test case corresponding to $\Delta p = 100$.

In [8], the authors test the first five problems using three types of DRP solvers with only partial success. Since no exact solutions are known, the reference solutions are obtained numerically, by solving the test problems on very fine mesh on the interval $[-1, 1] \times [0, t_0]$ of (x, t). To do this, the authors of [8,18] suggest using the Random Choice Method or Weighted Average Flux Method to avoid the large nonphysical oscillations of early time solution. To this aspect, a detailed description can be found in [8,18], which is beyond the scope of this work. Here, our numerical reference solutions are obtained simply by using the Godunov flux in the context of finite volume method and then correcting their values on the early time interval $[0, t_0/20]$ using an interpolation method. Such a measure does not affect our accuracy tests.

For each of these tests, we will compare the GRP solver based solution at the interface $x = 0$, as a function of time determined by (2.13), with the *reference numerical solution*. As will be shown below, the present GRP solvers are truly accurate, having the expected accuracy not only for all the test cases in [8], but also for cases with much larger initial jump in state variables.

7.1. Acoustic case with continuous state and jump in derivatives

This test is subject to the following initial conditions

$$\begin{aligned}
&\rho_L(x,0) = 1 + 0.56431x + 2.62896x^2,\\
&u_L(x,0) = 0.03125 - 1.024x + 1.92x^2,\\
&p_L(x,0) = 10 - 0.216x + 1.08x^2,\\
&\rho_R(x,0) = 1 + 2.04204x,\\
&u_R(x,0) = 0.03125 - 0.25x + 0.75x^2,\\
&p_R(x,0) = 10,
\end{aligned} \tag{7.1}$$

that are indeed the initial conditions used as Test 2 in [8] with slight modification, keeping only the same leading terms up to second order at $x = 0$. The initial condition (7.1) has a continuous state but with discontinuous derivatives at $x = 0$. The solution for this problem contains the left-going and the right-going acoustic waves. The t-axis is located in the intermediate region of the two acoustic waves. This test aims at testing the accuracy of the acoustic GRP solvers. Fig. 7.1 shows solutions of the LGRP_1 and QGRP_1 solvers by each component. The errors measured in L_∞ with the rates of convergence are displayed in Table 7.1.

7.2. Nonsonic case with jump in initial state

In this subsection, we test the GRP solvers in the nonsonic case with initial conditions having jump in state variables. The initial conditions are generated from (7.1) by adding a term in p_L and thus generating a jump $\Delta p = (P_L(0,0), P_R(0,0))/P_R(0,0)$ in pressure at $x = 0$.

The L_∞ errors of vector U with the convergence rates of the LGRP_∞ and QGRP_∞ solvers are tabulated in Tables 7.2 and 7.3, respectively. We can see that for all cases the LGRP_∞ attains order two and QGPR_∞ solver is essentially third order. For the QGRP solver, the decay of accuracy in some cases may be caused by the limited resolution of reference solution. Fig. 7.2 show the results of the acoustic LGRP_1 (resp. QGRP_1) solver in comparison with that of the LGRP_∞ (resp. QGRP_∞) solver with Δp ranging from 0.01 to 10. As Δp is small, the acoustic solvers do serve as good approximations of their counterpart ones. However, as the jump Δp increases, the performance of the acoustic solvers becomes worse. As $\Delta p = 10$, the acoustic solvers give absolutely wrong initial slopes. Indeed, the behaviors of the acoustic solvers are essentially the same as that of the approximate solvers studied in [8,18]. For even larger pressure jump cases $\Delta p = 100$ and $\Delta p = 1000$, the solutions profiles are shown in Fig. 7.3. We can see that, for all test cases, the LGRP_∞ and QGRP_∞ solvers based solutions agree well with the reference solutions.

7.3. Sonic case

For the sonic case, the test problem is generated by adding $\Delta u = 28$ on the initial velocity $u(x, 0)$ of the generalized Riemann problem in previous section corresponding to $\Delta p = 100$. Compared to the previous tests, it is more difficult to

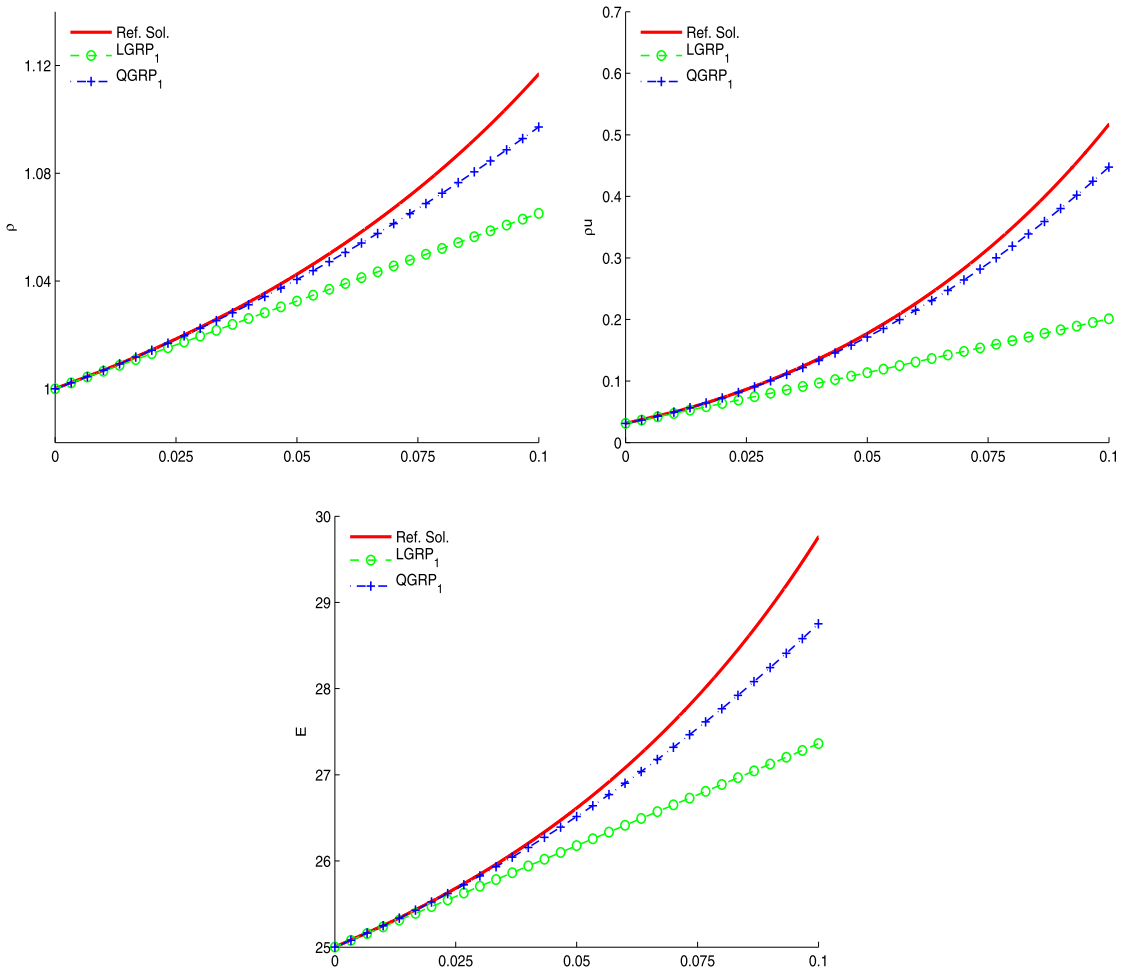

Fig. 7.1. Acoustic case: Reference solution and GRP solvers based solutions.

Table 7.1
The L_∞ errors of U and convergence rates of the acoustic GRP solvers.

Solver	$t = 0.1$		$t = 0.05$		$t = 0.025$		$t = 0.0125$	
	Error	Order	Error	Order	Error	Order	Error	Order
$LGRP_1$	2.420e+0	–	4.407e−1	2.46	9.592e−2	2.20	2.251e−02	2.09
$QGRP_1$	1.011e+0	–	9.861e−2	3.36	1.127e−2	3.13	1.439e−3	2.97

Table 7.2
The L_∞ errors of U and convergence rates of the $LGRP_\infty$ solvers: Nonsonic case.

Δp	t_0	$t = t_0$		$t = t_0/2$		$t = t_0/4$		$t = t_0/8$	
		Error	Order	Error	Order	Error	Order	Error	Order
0.01	0.1	2.456e+0	–	4.478e−1	2.46	9.762e−2	2.20	2.294e−2	2.09
0.1	0.1	2.782e+0	–	5.100e−1	2.45	1.115e−1	2.19	2.630e−2	2.08
1	0.1	6.012e+0	–	1.128e+0	2.41	2.507e−1	2.17	5.881e−2	2.09
10	0.05	5.823e+0	–	1.406e+0	2.05	3.515e−1	2.00	8.778e−2	2.00
100	0.01	1.265e+1	–	2.810e+0	2.17	6.501e−1	2.11	1.600e−1	2.02
1000	0.005	5.201e+2	–	1.277e+2	2.03	3.010e+1	2.08	7.300e+0	2.04

compute the reference solution for this case and we need to use a finer mesh with a smaller time interval. The reason is twofold. For the first, the solution is singular in the rarefaction wave, and for the second, we have observed an *aberration phenomenon* when computing reference solution. The aberration phenomenon is illustrated by Figs. 7.4 and 7.5: the computed reference of ψ_+ (or E) exhibits a *weak discontinuity point* and an *aberration region*. However, for the GRI S and ψ_-, such a phenomenon is not observed. This phenomenon is different from the afore-mentioned early-time oscillation [8],

Table 7.3
The L_∞ errors of U and convergence rates of the QGRP$_\infty$ solvers: Nonsonic case.

Δp	t_0	$t = t_0$		$t = t_0/2$		$t = t_0/4$		$t = t_0/8$	
		Error	Order	Error	Order	Error	Order	Error	Order
0.01	0.1	1.024e+0	–	9.997e−2	3.32	1.157e−2	3.11	1.517e−3	2.93
0.1	0.1	1.141e+0	–	1.113e−1	3.36	1.278e−2	3.12	1.721e−3	2.89
1	0.1	2.289e+0	–	2.250e−1	3.35	2.714e−2	3.05	3.105e−3	3.13
10	0.05	1.729e−1	–	2.035e−2	3.09	3.411e−3	2.58	7.979e−4	2.10
100	0.01	3.350e+0	–	4.900e−1	2.77	7.000e−2	2.81	1.000e−2	2.81
1000	0.005	8.220e+1	–	1.850e+1	2.15	2.800e+0	2.72	4.000e−1	2.81

since it is GRI-dependent. As the mesh is refined, the weak discontinuous point converges to the singularity $(0, 0)$ and the numerical solution converges.

This phenomenon can be viewed as a numerical justification of the fact that the second time derivative of a state variable, expect for the GRI, takes infinite value at the singularity. See Section 5.2.

The errors in terms of the vector $\Phi = (S, \psi_-, \psi_+)$ and the convergence rates of the GRP solvers are displayed in Table 7.4. As suggested in Section 5.2, for resolving the sonic case, we use the Newton iteration method with initial gauss $\beta = 0$ to solve (5.14). Here, for the tolerance $TOL = 1.0\text{e}{-7}$, the number of iterations required for convergence is no more than three.

8. Numerical schemes

In this section, we turn using GRP solvers to construct one step high order numerical schemes, namely, the GRP schemes. In the introduction section, we have described the process of implementing the second-order numerical scheme, where the LGRP solver provides a second-order approximation of the flux function from a piecewise linear discontinuous initial data.

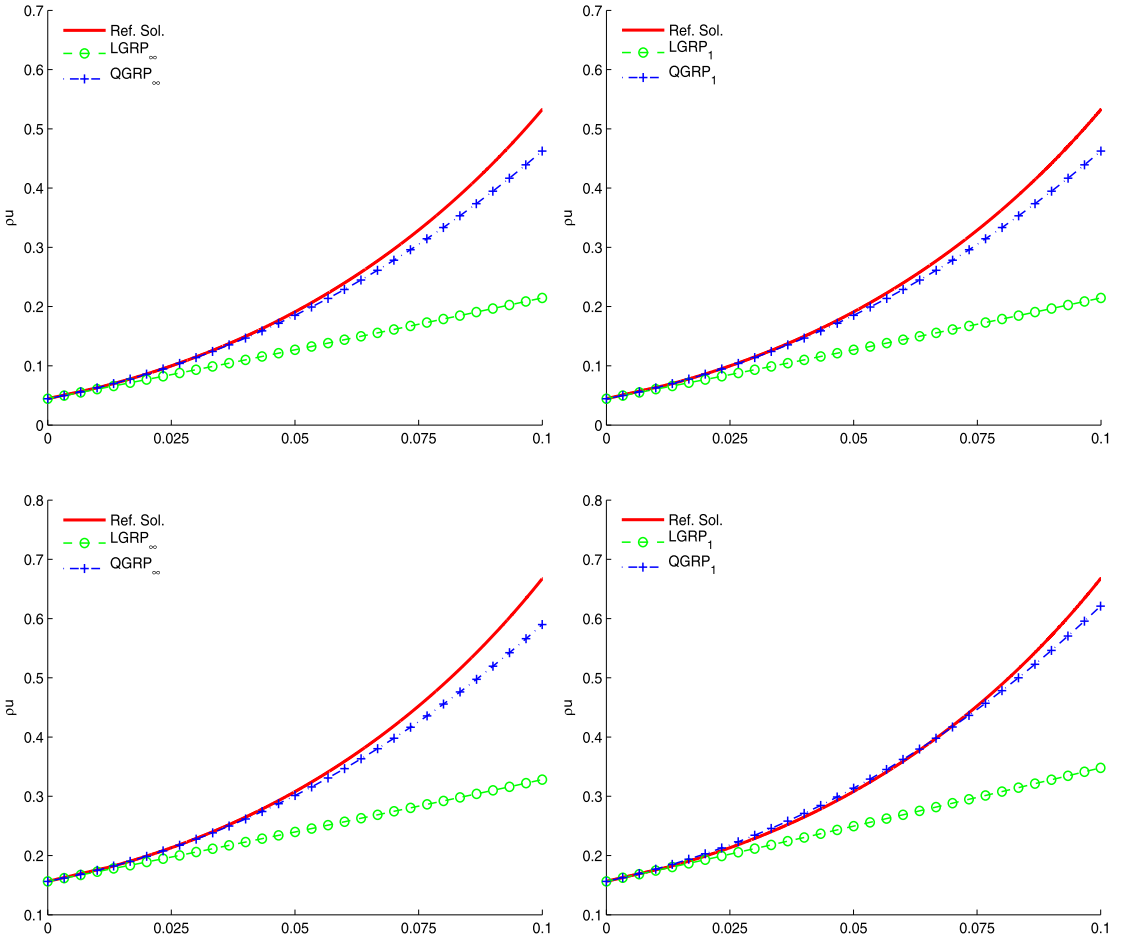

Fig. 7.2. Nonsonic case: Reference solution and GRP solvers based solutions. Left: LGRP$_\infty$ and LGRP$_\infty$ solvers; Right: LGRP$_1$ and LGRP$_1$ solvers. From top to bottom: $\Delta p = 0.01$, $\Delta p = 0.1$, $\Delta p = 1$, $\Delta p = 10$ (*continued on next page*).

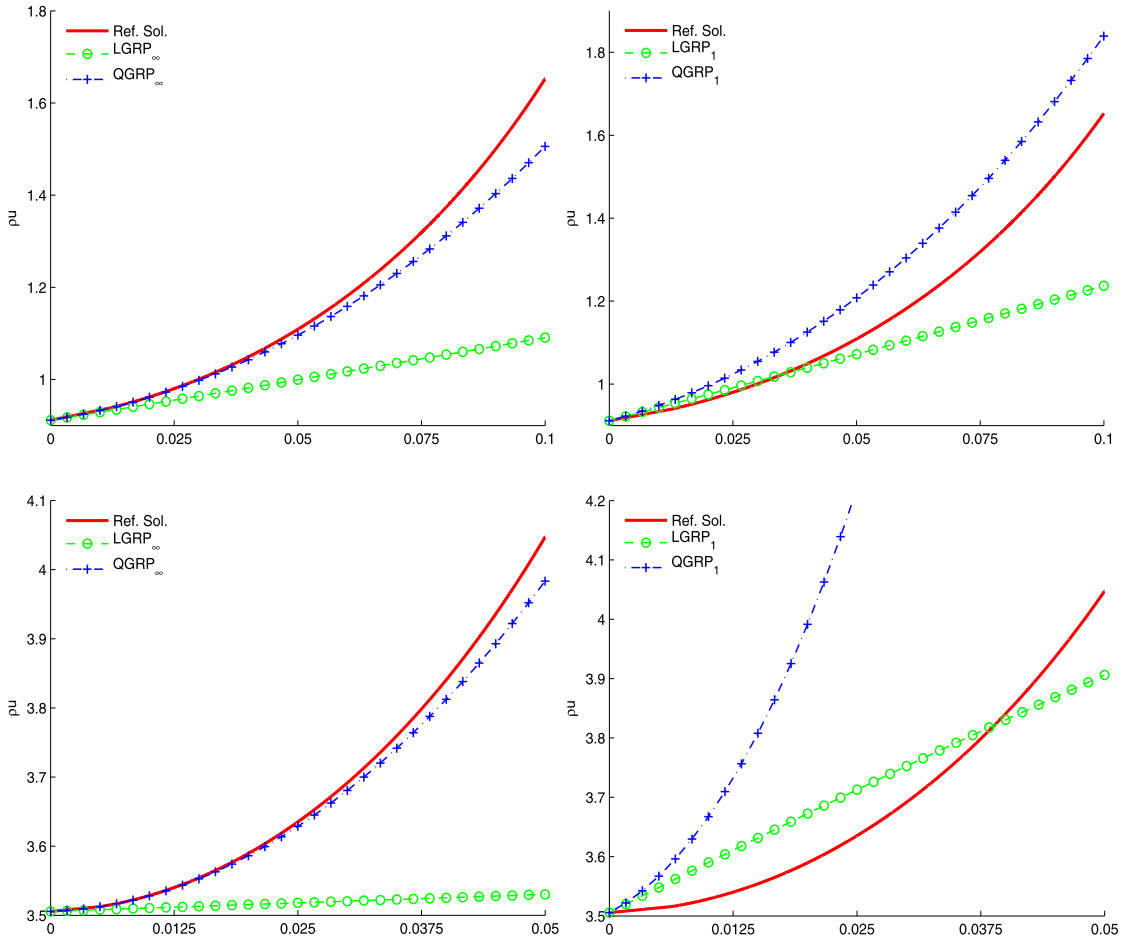

Fig. 7.2. (*continued*)

Table 7.4
The L_∞ errors of Φ and convergence rates of the GRP$_\infty$ solvers: Sonic case.

Solver	$t = t_0$		$t = 2/3t_0$		$t = t_0/2$		$t = 1/3t_0$	
	Error	Order	Error	Order	Error	Order	Error	Order
LGRP$_\infty$	1.114e+1	–	4.809e+0	2.06	2.671e+0	2.06	1.165	2.05
QGRP$_\infty$	1.052e+0	–	3.208e−1	3.13	1.304e−1	3.13	4.006e−2	2.91

The process of implementing the QGRP solver based third-order numerical scheme is similar. The difference is that we need to provide a third-order subcell data reconstruction on each time step and use two point quadrature for the integral in (1.3) to compute the numerical flux, i.e.,

$$F_{j+1/2} = \omega_1 F\big(U(x_{j+1/2}, \tau_1)\big) + \omega_2 F(x_{j+1/2}, \tau_2). \tag{8.7}$$

On each quadrature points $(x_{j+1/2}, \tau_i)$, the vector U is calculated through (2.13), wherein the time derivatives of U are determined by solving a generalized Riemann problem on the cell interface using the QGRP solver.

In the following, we present several one-dimensional examples to test the performance of our schemes. The uniform size meshes are used for all the test cases. For the second-order scheme, the van Leer limiter [25] is used to perform the linear reconstruction. For the third-order scheme, we use the same reconstruction method as in [17]. In fact, we use the fifth order WENO technique to reconstruct pointwise variables of U at each cell interface. Then based on the cell interface values and the cell averages of U_j^n, a third-order polynomial is constructed as the subcell flow distributions at time t^n. In the following numerical examples, the WENO reconstruction is carried out based on the characteristic decomposition [19] and the CFL number is set to be 0.5.

For all the problems, the GRP solutions are plotted against the exact solutions. The solid lines represent the exact solution, the circles show the second-order scheme solution, while the crosses stand for the solution by the third-order scheme.

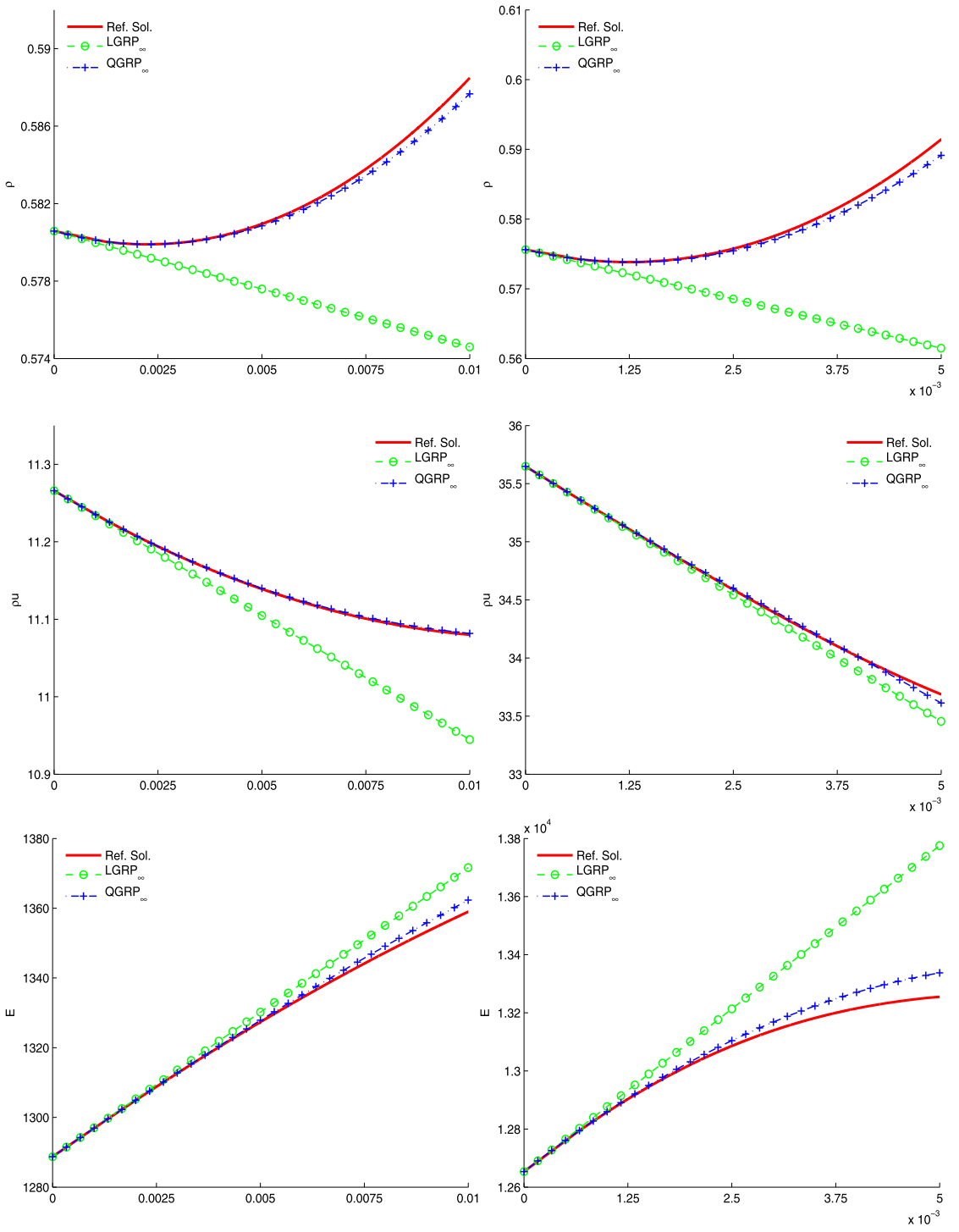

Fig. 7.3. Nonsonic case: Reference solution and GRP solvers based solutions. Left: $\Delta p = 100$; Right: $\Delta p = 1000$.

8.1. Sod problem

The first test is the standard Riemann problem proposed by Sod [21]. The gas is initially at rest with $\rho = 1$, $p = 1$ for $-5 \leqslant x < 0$ and $\rho = 0.125$, $p = 0.1$ for $0 \leqslant x < 5$. At time $t = 2$, the numerical solutions with 100 points are shown in Fig. 8.1. We can see that both of the computed solution agree well with the exact one and the third-order scheme shows better performance.

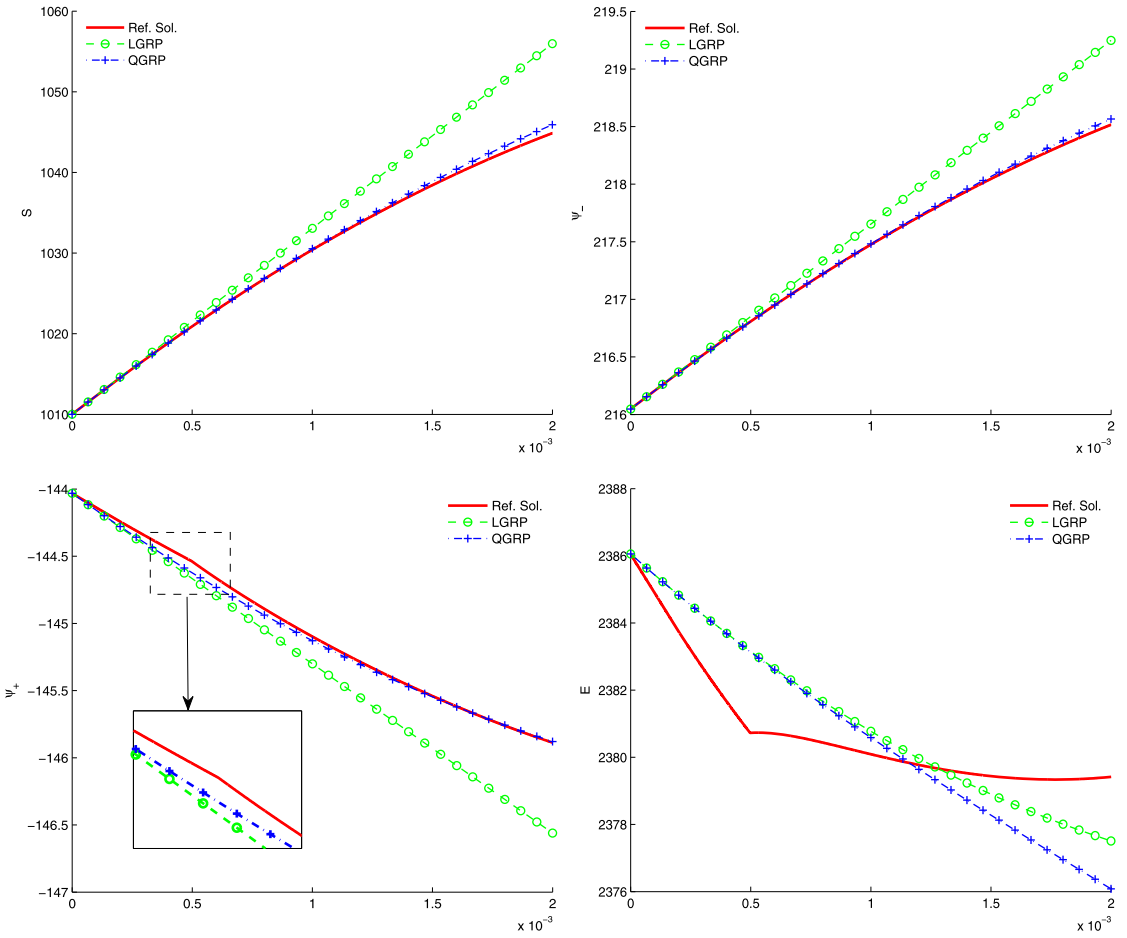

Fig. 7.4. Sonic case: Reference solution and GRP solvers based solutions. Uniform meshes of 2.0e−4 cell size are used for computing the reference solution.

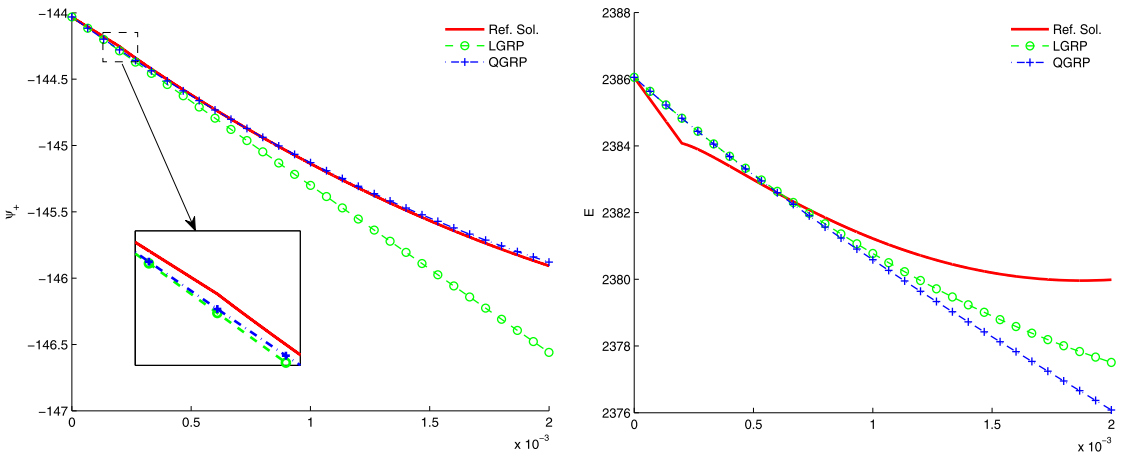

Fig. 7.5. Sonic case: Reference solution and GRP solvers based solutions. Uniform meshes of 2.5e−5 cell size are used for computing the reference solution.

8.2. 123 problem

This example was first proposed in [9]. The initial data is given with $(\rho, u, p) = (1, 2, 0.4)$ for $-5 \leqslant x < 0$ and $(\rho, u, p) = (1, 2, 0.4)$ for $0 \leqslant x < 5$. The numerical solutions at time $t = 1.2$ are shown in Fig. 8.2. This test case demonstrates the ability of the GRP scheme to preserve the positivity of the density, pressure and internal energy. Again, the internal energy profile conforms the better performance of third-order scheme.

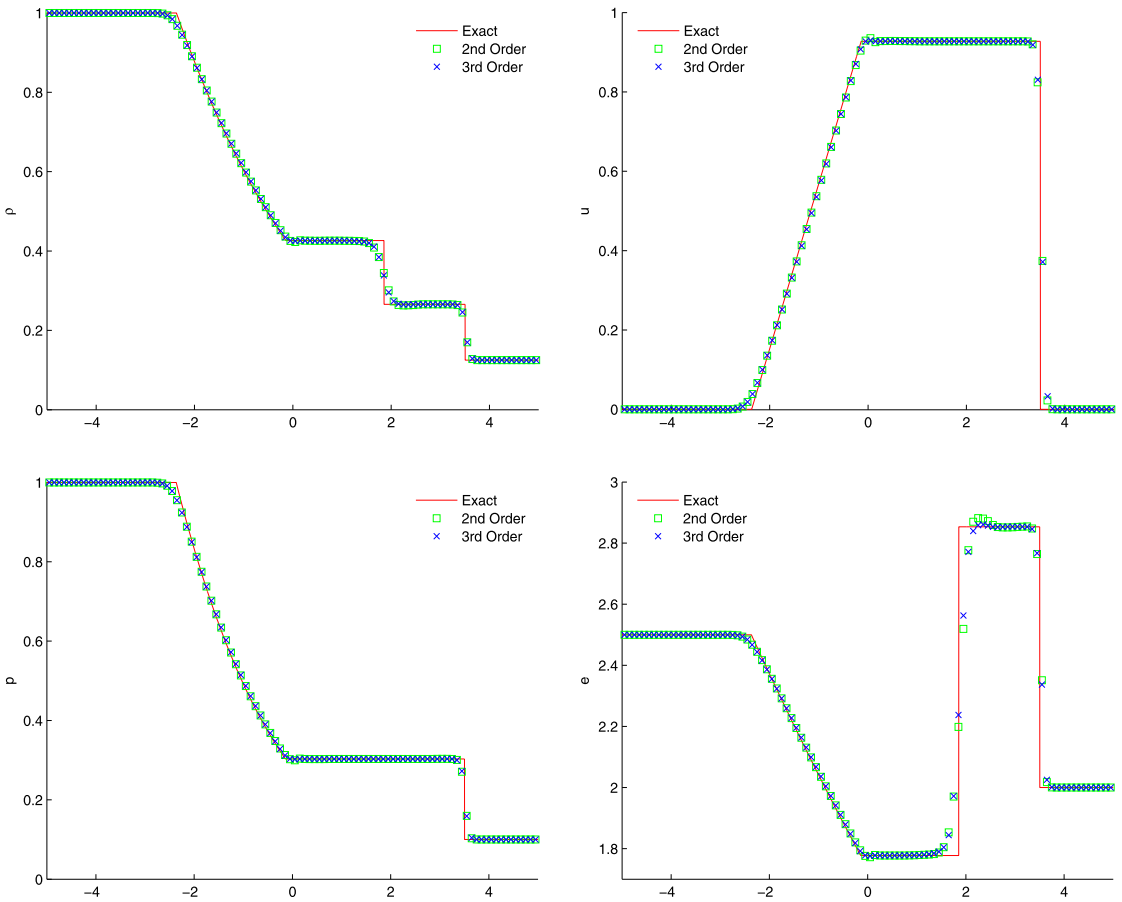

Fig. 8.1. Numerical solutions of the Sod problem: 100 grid points are used.

8.3. Woodward–Colella blast wave problem

This is a problem proposed in [26]. The diatomic gas is initially at rest, and the density is unit everywhere. The pressure is $p = 1000$ for $0 \leqslant x < 10$ and $p = 100$ for $90 \leqslant x < 100$, while it is only $p = 0.01$ in $10 \leqslant x < 90$. Reflecting boundary conditions are applied at both ends and the output time is $t = 3.8$. Numerical solutions with 400 points are shown in Fig. 8.3 to exhibit the performance of both schemes. This test case clearly demonstrates the capability of both schemes in the capturing of strong shock waves. The third-order scheme capture much sharper solution than the second-order scheme in the density and internal energy distribution.

8.4. Shock–density wave interaction

The Mach 3 shock–entropy wave interaction in [20] is specified by the initial condition: $(\rho, u, p) = (3.57134, 2.629369, 10.33333)$ for $0 \leqslant x < 1$ and $(\rho, u, p) = (1 + 0.2\sin(kx), 0, 1)$ for $1 \leqslant x \leqslant 10$ with $k = 5$. The solution of this problem consists of a number of shocklets and fine scale structures which are located behind a right-going main shock. The computed density profile with 400 points, at $t = 2.0$, is shown in Fig. 8.4. Again the third-order scheme works better and captures much finer scale structures at high frequency waves behind the shock.

8.5. Steady flow in a converging–diverging nozzle

We now use the examples in [4, Sect. 6.5] to test the ability of the GRP schemes to attain the steady state of a flow. Consider a flow in a converging–diverging nozzle, which occupies the internal $0 \leqslant x \leqslant 1$ and has a smooth cross-sectional area function $A(x)$ given by the following expression:

$$A(x) = \begin{cases} A_{\text{in}} \exp(-\log(A_{\text{in}}) \sin^2(2\pi x)), & 0 \leqslant x < 0.25; \\ A_{\text{ex}} \exp(-\log(A_{\text{ex}}) \sin^2(\frac{2\pi(1-x)}{3})), & 0.25 \leqslant x \leqslant 1, \end{cases} \tag{8.8}$$

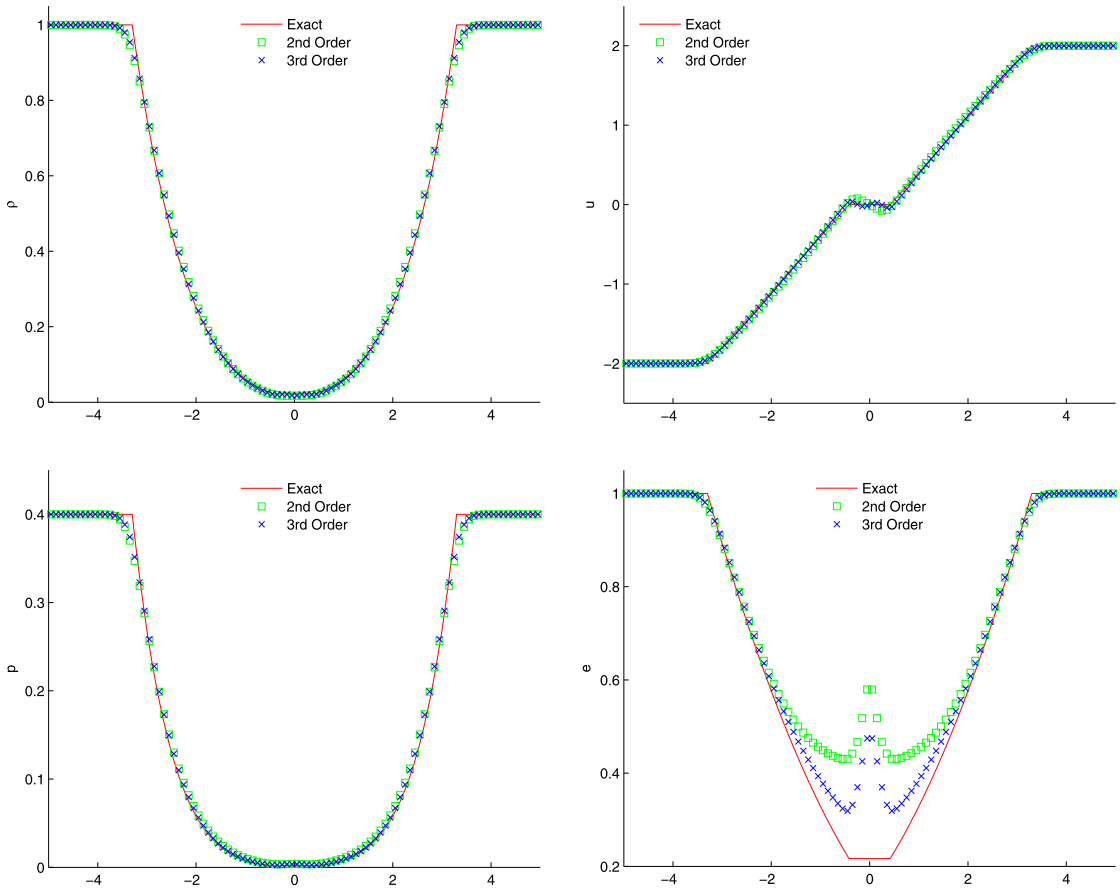

Fig. 8.2. Numerical solutions of the 123 problem. 100 grid points are used.

where $A_{\text{in}} = 4.8643$ and $A_{\text{ex}} = 4.2346$. See Fig. 8.5. For a steady duct flow of a perfect gas, the Mach number $M(x) = u(x)/c(x)$ is determined by $A(x)$ through the algebraic relation

$$\big[A(x)\big]^2 = \frac{1}{[M(x)]^2}\left[\frac{2}{\gamma+1}\left(1+\frac{\gamma-1}{2}\big[M(x)\big]^2\right)\right]^{\frac{\gamma+1}{\gamma-1}}. \tag{8.9}$$

Then the steady flow profiles in the nozzle are given by

$$\begin{aligned} p(x) &= p_0\left(1+\frac{\gamma-1}{2}\big[M(x)\big]^2\right)^{-\frac{\gamma}{\gamma-1}}, \\ \rho(x) &= \rho_0\left(1+\frac{\gamma-1}{2}\big[M(x)\big]^2\right)^{-\frac{1}{\gamma-1}}, \\ u(x) &= M(x)\sqrt{\gamma\, p(x)/\rho(x)}, \end{aligned} \tag{8.10}$$

for the smooth flow, where ρ_0 and p_0 need to be specified.

The initial data we use are

$$U(x,0) = \begin{cases} U_L = (\rho_0, 0, p_b), & 0 < x < 0.25, \\ U_R = (\rho_0(p_b/p_0)^{1/\gamma}, 0, p_b), & 0.25 < x < 1, \end{cases} \tag{8.11}$$

where p_b is a constant determined by the steady state solution at $x = 1$. We consider two cases. In both cases we take $\rho_0 = p_0 = 0$ and $A(x)$ as in (8.8).

(A) A smooth flow where $p(1) = 0.0272237$ is obtained from (8.10) by taking $x = 1$ in (8.9), leading to $M(1) = 3$.
(B) Setting $p(1) = 0.4$ leads to a discontinuous steady state solution, as shown by solid lines in Fig. 8.8.

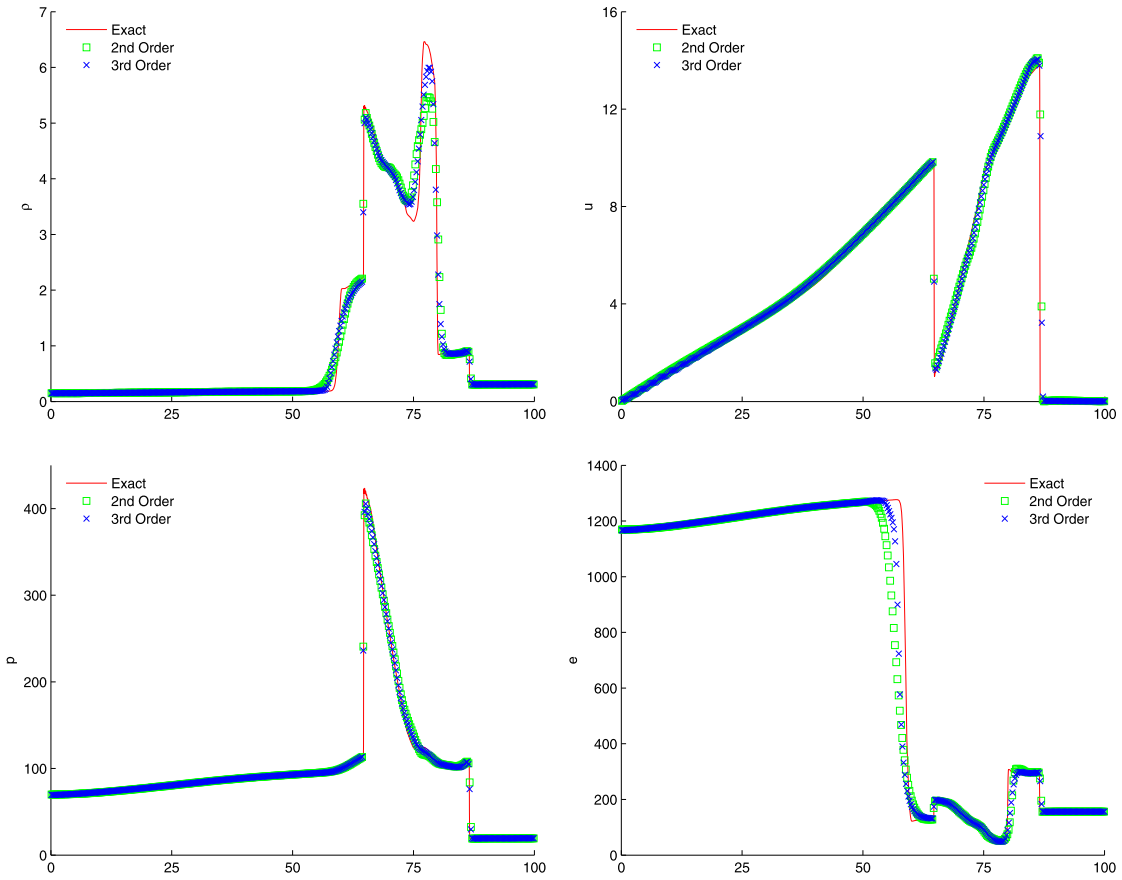

Fig. 8.3. Numerical solutions of the Woodward–Colella blast problem. 400 grids point are used.

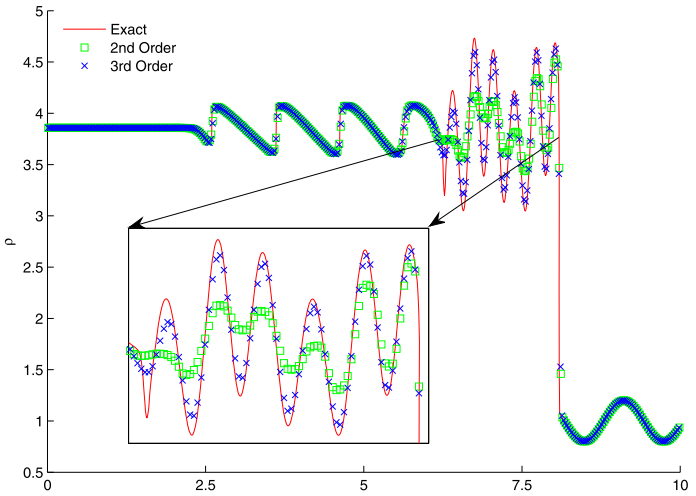

Fig. 8.4. Numerical solutions of the shock–density wave problem. 400 grid point are used.

We use the strategy in [4, Sect. 6.5] to deal with the boundary conditions at $x = 0$ and 1. In both cases, the number of grid points used are 22. As shown in Figs. 8.6 and 8.8, both of the GRP solutions at $t = 15.5$ are good agreement with the exact solution. The third-order GRP solutions are closer to the analytical solutions than the second-order ones. Moreover, as shown in Fig. 8.7, the GRP solutions almost attain the steady state at time $t = 2.5$. This shows that the GRP solutions converges to steady solution quickly.

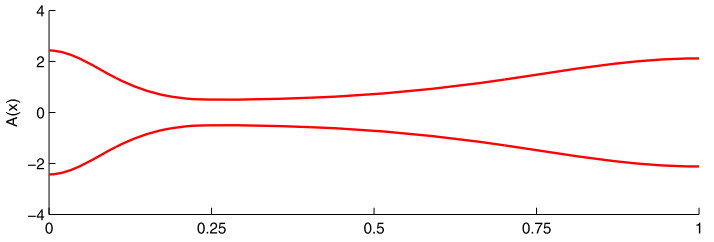

Fig. 8.5. Nozzle contour.

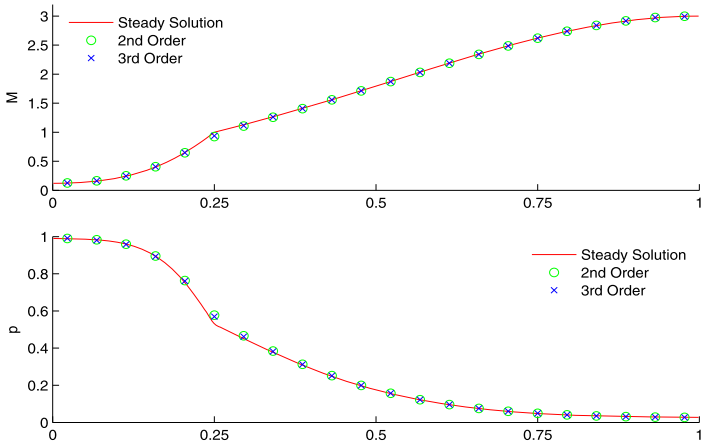

Fig. 8.6. Large time flow in Laval nozzle at time $t = 15.5$: Case A. 22 grid points are used.

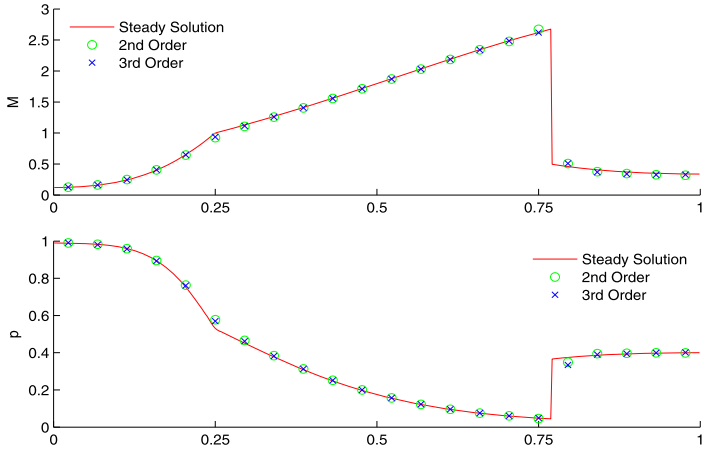

Fig. 8.7. Large time flow in Laval nozzle at time $t = 2.5$: Case B. 22 grid points are used.

Appendix A. Formulae in Section 3

The functions $Z_1^\gamma(\beta)$ and $Z_2^\gamma(\beta)$ in Lemma 3.3 are as follows: for $\gamma \neq 3, 5/3$,

$$Z_1^\gamma(\beta) = \frac{2(\gamma-1)}{3\gamma-1} A_{15}(\psi_L-\beta)^{\frac{-3\gamma+1}{2(\gamma-1)}} - A_{16}\ln(\psi_L-\beta) + \frac{\gamma-1}{\gamma+1} C_1(\psi_L-\beta)^{-(\frac{\gamma+1}{\gamma-1})} + \frac{\gamma-1}{2} C_2(\psi_L-\beta)^{\frac{-2}{\gamma-1}},$$

$$Z_2^\gamma(\beta) = \frac{1}{2\gamma^2 S_L}(\psi_L-\beta)^{-\frac{2}{\gamma-1}} \frac{D_-^2 S}{Dt^2}(0,\beta) + \frac{\gamma-1}{\gamma+1}\left[\frac{A_{15}}{\gamma^2 S_L} - 2A_{17}\right](\psi_L-\beta)^{\frac{\gamma+1}{2(\gamma-1)}}$$

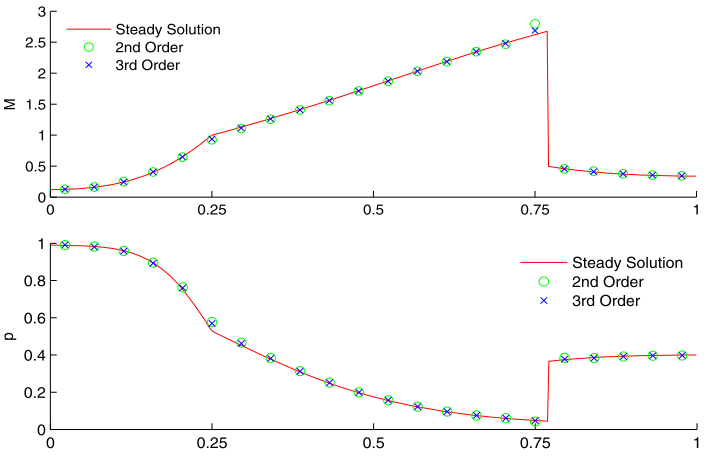

Fig. 8.8. Large time flow in Laval nozzle at time $t = 15.5$: Case B. 22 grid points are used.

$$
\begin{aligned}
&+\frac{\gamma-1}{2\gamma}\left[\frac{A_{16}}{2\gamma^2 S_L}-A_{18}\right](\psi_L-\beta)^{\frac{2\gamma}{\gamma-1}}+A_{19}(\psi_L-\beta)^{-1}\\
&+\left[\frac{C_1}{2\gamma^2 S_L}-C_4\right](\psi_L-\beta)+\left[\frac{C_2}{4\gamma^2 S_L}-\frac{C_6}{2}\right](\psi_L-\beta)^2\\
&+\frac{2(\gamma-1)}{\gamma+1}C_3(\psi_L-\beta)^{-\frac{\gamma+1}{2(\gamma-1)}}-\frac{2(\gamma-1)}{\gamma-3}C_5(\psi_L-\beta)^{\frac{\gamma-3}{2(\gamma-1)}}\\
&+\frac{\gamma-1}{2}C_7(\psi_L-\beta)^{-\frac{2}{\gamma-1}}-\frac{\gamma-1}{\gamma-3}C_8(\psi_L-\beta)^{\frac{\gamma-3}{\gamma-1}}-\frac{\gamma-1}{2(\gamma-2)}C_9(\psi_L-\beta)^{\frac{2(\gamma-2)}{\gamma-1}};
\end{aligned}
$$

for $\gamma = 3$,

$$
\begin{aligned}
Z_1^3(\beta) &= \left(\frac{X_1}{2}+\frac{X_4}{4}\right)(\psi_L-\beta)^{-2}-X_2(\psi_L-\beta)^{-1}-X_3\ln(\psi_L-\beta)+\frac{X_4}{2}(\psi_L-\beta)^{-2}\ln(\psi_L-\beta),\\
Z_2^3(\beta) &= \frac{1}{18S_L}(\psi_L-\beta)^{-1}\frac{D_-^2 S}{Dt^2}(0,\beta)+(X_5+X_{10}+2X_{13})(\psi_L-\beta)^{-1}\\
&\quad+\left(\frac{X_1}{54S_L}-\frac{X_4}{54S_L}+X_{12}-X_7\right)(\psi_L-\beta)+\left(\frac{X_2}{27}-\frac{X_8}{2}\right)(\psi_L-\beta)^2+\left(\frac{X_3}{486}-\frac{X_9}{3}\right)(\psi_L-\beta)^3\\
&\quad+\left[(2X_{13}+X_{10})(\psi_L-\beta)^{-1}-Z_6+\left(\frac{X_4}{54}-X_{12}\right)(\psi_L-\beta)\right]\ln(\psi_L-\beta)\\
&\quad+\left[X_{13}(\psi_L-\beta)^{-1}-X_{11}\right]\ln^2(\psi_L-\beta);
\end{aligned}
$$

and for $\gamma = 5/3$,

$$
\begin{aligned}
Z_1^{5/3}(\beta) &= \frac{Y_1}{4}(\psi_L-\beta)^{-4}-\frac{Y_2}{3}(\psi_L-\beta)^{-3}\\
&\quad+\frac{Y_4}{2}(\psi_L-\beta)^{-2}-Y_3\ln(\psi_L-\beta)+\frac{Y_4}{3}(\psi_L-\beta)^{-3}\ln(\psi_L-\beta),\\
Z_2^{5/3}(\beta) &= \frac{9}{50S_L}(\psi_L-\beta)^{-3}\frac{D_-^2 S}{Dt^2}(0,\beta)+\frac{Y_5}{3}(\psi_L-\beta)^{-3}\\
&\quad+\left(\frac{Y_6}{2}+\frac{Y_{11}}{4}\right)(\psi_L-\beta)^{-2}+(Y_7+Y_{12}+2Y_{14})(\psi_L-\beta)^{-1}+\left(\frac{9Y_1}{50S_L}-\frac{Y_{10}}{5}\right)(\psi_L-\beta)^5\\
&\quad+\left[\frac{Y_{11}}{2}(\psi_L-\beta)^{-2}+(2Y_{14}+Y_{12})(\psi_L-\beta)^{-1}+\left(\frac{9Y_4}{100S_L}-\frac{Y_{13}}{2}\right)(\psi_L-\beta)^2\right]\ln(\psi_L-\beta)\\
&\quad+Y_{14}(\psi_L-\beta)^{-1}\ln^2(\psi_L-\beta).
\end{aligned}
$$

Table A.1
The coefficients $A_3, \ldots, A_{19}$ and $B_1, \ldots, B_{12}$.

A_3	$\frac{1}{\gamma(3\gamma-1)S_L}A_1$	B_1	$\frac{\gamma-1}{\gamma-3}\psi_L\frac{A'(x)}{A(x)}$
A_4	$-\frac{1}{\gamma(\gamma+1)S_L}A_1$	B_2	$-\frac{2(\gamma-1)}{(\gamma+1)(3\gamma-5)}\frac{A'(x)}{A(x)}$
A_5	$\frac{\gamma-1}{4}A_2$	B_3	$\frac{\gamma-1}{\gamma+1}\psi_L\frac{A'(x)}{A(x)}$
A_6	$\frac{\gamma-1}{4}(A_3-A_4)$	B_4	$-\frac{2(\gamma-1)}{(\gamma+1)^2}\frac{A'(x)}{A(x)}$
A_7	$-\frac{(3-\gamma)(\gamma+1)}{8(\gamma-1)}A_2$	B_5	$\frac{\gamma-1}{4}(B_1-B_3)$
A_8	$-\frac{2\gamma}{\gamma-1}(\frac{3-\gamma}{4}A_3+\frac{1+\gamma}{4}A_4)$	B_6	$\frac{\gamma-1}{4}(B_2-B_4)$
A_9	$\frac{1}{\gamma(\gamma-1)S_L^2}A_1$	B_7	$-\frac{3-\gamma}{4}B_1-\frac{\gamma+1}{4}B_3$
A_{10}	$-\frac{1}{2\gamma(\gamma-1)S_L}A_7$	B_8	$-\frac{3-\gamma}{2}B_2-\frac{\gamma+1}{2}B_4$
A_{11}	$-\frac{1}{2\gamma(\gamma-1)S_L}A_8$	B_9	$\frac{1}{2}(\frac{\gamma+1}{\gamma-1})^2B_5-\frac{\gamma+1}{2(\gamma-1)}B_7$
A_{12}	$(\frac{\gamma+1}{\gamma-1})^2A_5-\frac{\gamma+1}{2(\gamma-1)}A_7$	B_{10}	$\frac{1}{2}(\frac{\gamma+1}{\gamma-1})^2B_6-\frac{\gamma+1}{2(\gamma-1)}B_8$
A_{13}	$(\frac{\gamma+1}{\gamma-1})^2A_6-\frac{\gamma+1}{2(\gamma-1)}A_8$	B_{11}	$-\frac{1}{2\gamma(\gamma-1)S_L}B_7$
A_{14}	A_9+A_{11}	B_{12}	$-\frac{1}{2\gamma(\gamma-1)S_L}B_8$
A_{15}	$2A_1A_{12}$		
A_{16}	$2A_1A_{13}$		
A_{17}	$A_1A_{10}+A_2A_{13}+A_3A_{12}$		
A_{18}	$A_1A_{14}+A_3A_{13}$		
A_{19}	A_2A_{12}		

Table A.2
The coefficients $C_1, \ldots, C_9$.

C_1	$2A_1B_9$
C_2	$2A_1B_{10}$
C_3	$A_2B_9+A_{12}B_1-\frac{\psi_L}{2}A_7\frac{A'(x)}{A(x)}$
C_4	$A_3B_9+A_1B_{11}+A_{13}B_1-\frac{\psi_L}{2}A_8\frac{A'(x)}{A(x)}$
C_5	$A_2B_{10}+A_{12}B_2+(\frac{A_7}{\gamma+1}-\frac{A_2}{2})\frac{A'(x)}{A(x)}$
C_6	$A_3B_{10}+A_1B_{12}+A_{13}B_2+(\frac{A_8}{\gamma+1}-\frac{A_3+A_4}{2})\frac{A'(x)}{A(x)}$
C_7	$B_1B_9-\frac{\psi_L}{2}B_7\frac{A'(x)}{A(x)}-\psi_L^2(\frac{A'(x)}{A(x)})'$
C_8	$B_2B_9+B_1B_{10}+(-\frac{\psi_L}{2}B_8+\frac{B_7}{\gamma+1}-\frac{B_1+B_3}{2})\frac{A'(x)}{A(x)}+\frac{\gamma+3}{\gamma+1}\psi_L(\frac{A'(x)}{A(x)})'$
C_9	$B_2B_{10}+(-\frac{B_8}{\gamma+1}-\frac{B_2+B_4}{2})\frac{A'(x)}{A(x)}-\frac{2}{\gamma+1}(\frac{A'(x)}{A(x)})'$

Table A.3
The coefficients $X_1, \ldots, X_{13}$.

X_1	$2A_1(2A_1-B_2)$
X_2	$2A_1B_2$
X_3	$2A_1(2A_3+A_4)$
X_4	$2\psi_LA_1\frac{A'(x)}{A(x)}$
X_5	$2A_2(A_2-B_3)-B_3(A_2-\frac{\psi_L}{2}\frac{A'(x)}{A(x)})-\psi_L^2(\frac{A'(x)}{A(x)})'$
X_6	$A_2(2B_2+B_4)-(\frac{A_2}{2}+\psi_LB_4)\frac{A'(x)}{A(x)}+\frac{3}{2}\psi_L(\frac{A'(x)}{A(x)})'$
X_7	$2A_2(A_3+A_4)+B_2(B_2+B_4)+A_3(\frac{A_1}{12S_L}-2B_3)$ $+\frac{1}{2}(B_4-B_2-3\psi_LA_4)\frac{A'(x)}{A(x)}+\frac{1}{2}(\frac{A'(x)}{A(x)})'$
X_8	$A_3(B_2+B_3)+2A_4(B_2-B_4)+B_4(\frac{A_1}{6S_L}+A_3)+\frac{1}{2}(2A_4-A_3)\frac{A'(x)}{A(x)}$
X_9	$A_3(A_3-4A_4)+\frac{1}{4S_L}A_1A_4$
X_{10}	$\frac{\psi_L}{2}(4A_1-B_3)\frac{A'(x)}{A(x)}$
X_{11}	$\frac{\psi_L}{4}(8B_2-\frac{A'(x)}{A(x)})\frac{A'(x)}{A(x)}$
X_{12}	$\frac{\psi_L}{2}(2A_3+A_4)\frac{A'(x)}{A(x)}$
X_{13}	$\frac{\psi_L^2}{2}(\frac{A'(x)}{A(x)})^2$

In Lemma 3.3, Remark 3.2 and the above formulae for $Z_1^\gamma(\beta)$ and $Z_2^\gamma(\beta)$, the coefficients A_i, B_j, C_k, X_l and Y_m are defined as in Tables A.1–A.4.

Table A.4
The coefficients $Y_1, \ldots, Y_{14}$.

Y_1	$\frac{4}{3}A_1(5B_1 - B_2)$
Y_2	$8A_1A_2 - \frac{A_1}{2}\frac{A'(x)}{A(x)}$
Y_3	$12A_3 + 8A_4$
Y_4	$-3A_1\frac{A'(x)}{A(x)}$
Y_5	$\frac{2}{3}B_1(5B_1 - 2B_1) + \frac{\psi_L}{2}(B_1 + 2B_2)\frac{A'(x)}{A(x)} - \psi_L^2(\frac{A'(x)}{A(x)})'$
Y_6	$\frac{22}{3}A_2B_1 - \frac{4}{3}A_2B_2 + \frac{7}{4}\psi_L + (\frac{\psi_L}{3}A_2 + \frac{2\psi_L}{3}B_4 - \frac{7}{8}B_1 - \frac{3}{4}B_2)\frac{A'(x)}{A(x)} - \frac{\psi_L}{16}(\frac{A'(x)}{A(x)})^2$
Y_7	$4A_2^2 - (A_2 + B_4)\frac{A'(x)}{A(x)} + \frac{3}{64}(\frac{A'(x)}{A(x)})^2 - \frac{3}{4}(\frac{A'(x)}{A(x)})'$
Y_8	$2A_3(B_1 - 2B_2) + 2B_1(3A_3 + 2A_4) - \frac{3}{20S_L}A_1(B_1 + 2B_2) + \frac{5\psi_L}{6}(A_3 + 2A_4)\frac{A'(x)}{A(x)}$
Y_9	$2A_2^2 + \frac{8}{3}A_2A_4 - (\frac{11}{8}A_3 + \frac{7}{4}A_4)\frac{A'(x)}{A(x)} + \frac{1}{18S_L}A_1(A_2 + 2B_4)$
Y_{10}	$\frac{1}{3}A_3(13A_3 - 2A_4) + \frac{5}{36S_L}A_1(A_3 + 2A_4)$
Y_{11}	$(-\frac{11}{4}B_1 + \frac{1}{2}B_2 - \frac{\psi_L}{8}\frac{A'(x)}{A(x)})\frac{A'(x)}{A(x)}$
Y_{12}	$(-3A_2 + \frac{3}{16}\frac{A'(x)}{A(x)})\frac{A'(x)}{A(x)}$
Y_{13}	$-(\frac{15}{4}A_3 + \frac{3}{2}A_4 + \frac{A_1}{48S_L})\frac{A'(x)}{A(x)}$
Y_{14}	$\frac{9}{16}(\frac{A'(x)}{A(x)})^2$

References

[1] M. Ben-Artzi, The generalized Riemann problem for reactive flows, J. Comput. Phys. 81 (1) (1989) 70–101.
[2] M. Ben-Artzi, J. Falcovitz, A second-order Godunov-type scheme for compressible fluid dynamics, J. Comput. Phys. 55 (1) (1984) 1–32.
[3] M. Ben-Artzi, J. Falcovitz, An upwind second-order scheme for compressible duct flows, SIAM J. Sci. Stat. Comput. 7 (3) (1986) 744–768.
[4] M. Ben-Artzi, J. Falcovitz, Generalized Riemann Problems in Computational Fluid Dynamics, Cambridge Monographs on Applied and Computational Mathematics, vol. 11, 2003.
[5] M. Ben-Artzi, J. Li, Hyperbolic balance laws: Riemann invariants and the generalized Riemann problem, Numer. Math. 106 (2007) 369–425.
[6] M. Ben-Artzi, J. Li, G. Warnecke, A direct Eulerian GRP scheme for compressible fluid flows, J. Comput. Phys. 218 (2006) 19–34.
[7] A. Bourgeade, P. LeFloch, P.A. Raviart, An asymptotic expansion for the solution of the generalized Riemann problem. II. Application to the equations of gas dynamics, Ann. Inst. Henri Poincaré, Anal. Non Linéaire 6 (6) (1989) 437–480.
[8] C.E. Castro, E.F. Toro, Solvers for the high-order Riemann problem for hyperbolic balance laws, J. Comput. Phys. 227 (2008) 2481–2513.
[9] B. Einfeldt, C.D. Munz, P.L. Roe, B. Sjögreen, On Godunov-type methods near low densities, J. Comput. Phys. 92 (1991) 273–295.
[10] S.K. Godunov, A finite-difference method for the numerical computation of discontinuous solutions of the equations of fluid dynamics, Mat. Sb. 47 (1959) 271–295.
[11] A. Harten, High resolution schemes for hyperbolic conservation laws, J. Comput. Phys. 49 (1983) 357–393.
[12] A. Harten, B. Engquist, S. Osher, S. Chakravarthy, Uniformly high order essentially non-oscillatory schemes III, J. Comput. Phys. 71 (1987) 231–303.
[13] P. LeFloch, P.-A. Raviart, An asymptotic expansion for the solution of the generalized Riemann problem. I. General theory, Ann. Inst. Henri Poincaré, Anal. Non Linéaire 5 (2) (1988) 179–207.
[14] J. Li, G. Chen, The generalized Riemann problem method for the shallow water equations with bottom topography, Int. J. Numer. Methods Eng. 65 (6) (2006) 834–862.
[15] J. Li, J. Qian, S. Wang, A genuinely multidimensional GRP solvers for compressible fluid flows, 2013, in preparation.
[16] Q. Li, K. Xu, Song Fu, A high-order gas-kinetic Navier–Stokes flow solver, J. Comput. Phys. 229 (2010) 6715–6731.
[17] J. Luo, L.J. Xuan, K. Xu, Comparison of fifth-order WENO scheme and WENO-gas-kinetic scheme for inviscid and viscous flow simulation, Commun. Comput. Phys. 14 (3) (2013) 599–620.
[18] G. Montecinos, C.E. Castro, M. Dumbser, E.F. Toro, Comparison of solver for the generalized Riemann problem for hyperbolic systems with source terms, J. Comput. Phys. 231 (2012) 6472–6494.
[19] C.W. Shu, Essentially Non-Oscillatory and Weighted Essentially Non-Oscillatory Schemes for Hyperbolic Conservation Laws, Lect. Notes Math., Springer, 1998.
[20] C.W. Shu, S. Osher, Efficient implementation of essentially non-oscillatory shock-capturing schemes, J. Comput. Phys. 77 (1988) 439–471.
[21] G.A. Sod, A survey of several finite difference methods for systems of nonlinear hyperbolic conservation laws, J. Comput. Phys. 27 (1978) 1–31.
[22] E.F. Toro, Riemann Solvers and Numerical Methods for Fluid Dynamics: A Practical Introduction, Springer, 1997.
[23] E.F. Toro, V.A. Tarev, Derivative Riemann solvers for systems for conservation laws and ADER methods, J. Comput. Phys. 212 (2006) 150–165.
[24] B. van Leer, Towards the ultimate conservative difference scheme II. Monotonicity and conservation combined in a second-order scheme, J. Comput. Phys. 14 (1974) 361–370.
[25] B. van Leer, Towards the ultimate conservative difference scheme, V. A second order sequel to Godunov's method, J. Comput. Phys. 32 (1979) 101–136.
[26] P. Woodward, P. Colella, The numerical simulation of two-dimensional fluid flow with strong shocks, J. Comput. Phys. 54 (1984) 115–173.
[27] Z.C. Yang, P. He, H.Z. Tang, A direct Eulerian GRP scheme for relativistic hydrodynamics: one-dimensional case, J. Comput. Phys. 230 (2011) 7964–7987.
[28] Z.C. Yang, H.Z. Tang, A direct Eulerian GRP scheme for relativistic hydrodynamics: Two-dimensional case, J. Comput. Phys. 231 (2012) 2116–2139.